

## LATE-STAGE CRYSTALLIZATION HISTORY OF THE JURASSIC NORTH MOUNTAIN BASALT, NOVA SCOTIA, CANADA. I. TEXTURAL AND CHEMICAL EVIDENCE FOR PERVASIVE DEVELOPMENT OF SILICATE-LIQUID IMMISCIBILITY

DANIEL J. KONTAK<sup>§</sup>

*Nova Scotia Department of Natural Resources, P.O. Box 698, Halifax, Nova Scotia B3J 2T9, Canada*

MICHELLE Y. DE WOLFE DE YOUNG

*Department of Earth Sciences, Laurentian University, Ramsey Lake Road, Sudbury, Ontario P3E 2C6, Canada*

JAROSLAV DOSTAL

*Department of Geology, St. Mary's University, Halifax, Nova Scotia B3H 3C3, Canada*

### ABSTRACT

The Jurassic (201 Ma) quartz-normative continental tholeiitic basalts of the North Mountain Basalt (NMB) Formation of southern Nova Scotia, Canada, record evidence of pervasive silicate-liquid immiscibility. The basalts, up to 400 m thick, typically with phenocrysts of plagioclase ( $An_{50-70}$ ) and clinopyroxene ( $Wo_{40}En_{40}Fs_{20}$ ), are subdivided into lower, middle, and upper units on the basis of the nature of the flows and petrographic features. Petrographic observations combined with image analysis indicate that the middle and upper units are characterized by an abundance of mesostasis material (*i.e.*, quenched residual melt) that contains skeletal clinopyroxene, acicular plagioclase, skeletal Fe–Ti oxides, Fe–Ti–P-rich globules, and andesitic to rhyolitic glass. Raster analysis of the mesostasis tracks an *in situ* fractionation that culminated in formation of an interstitial felsic glass (*i.e.*, 74 wt.%  $SiO_2$ ) that contains skeletal apatite and Fe-rich clinopyroxene. The composition of the skeletal clinopyroxene, *ca.*  $Wo_{20}En_{15}Fs_{65}$ , acicular plagioclase ( $An_{35-55}$ ,  $\leq 2.5$  wt.% FeO), Fe–Ti–P-rich globules, and intergranular glass of the mesostasis are consistent with formation from an interstitial melt that evolved in a disequilibrium environment promoted by rapid cooling of the lavas. The mineralogical and chemical features are consistent with the process of silicate-liquid immiscibility within the residual liquids of basaltic systems, in this case late-stage intergranular melts. The presence within the NMB of (1) Fe-rich clinopyroxene-bearing mafic pegmatite, (2) thin (*i.e.*, 1–2 cm) seams of rhyolite associated with the mafic pegmatites, and (3) locally abundant segregation pipes of mixed mafic–felsic composition, is considered to reflect mobilization of the Fe- and silica-rich immiscible melts.

*Keywords:* North Mountain Basalt, tholeiites, immiscibility, Bay of Fundy, Nova Scotia.

### SOMMAIRE

Les basaltes tholéïtiques continentaux de la Formation de North Mountain, du sud de la Nouvelle-Ecosse, au Canada, d'âge jurassique (201 Ma) et à quartz normatif, démontrent de l'évidence répandue d'une immiscibilité liquide. Les basaltes, atteignant une épaisseur de 400 m, possèdent typiquement des phénocristaux de plagioclase ( $An_{50-70}$ ) et de clinopyroxène ( $Wo_{40}En_{40}Fs_{20}$ ), et sont subdivisés en séquences inférieure, moyenne, et supérieure selon des critères pétrographiques et les aspects des coulées. Les observations pétrographiques, documentées avec traitement d'images, indiquent dans les unités du milieu et supérieure une abondance de mésostase (liquide résiduel trempé) dans lequel se trouvent clinopyroxène squelettique, plagioclase aciculaire, oxydes Fe–Ti squelettiques, globules enrichies en Fe–Ti–P, et un verre andésitique à rhyolitique. Une analyse de cette mésostase par balayage permet de suivre le fractionnement *in situ* qui a mené à la formation d'un verre interstitiel felsique (*i.e.*, 74%  $SiO_2$ , par poids) contenant de l'apatite squelettique et un clinopyroxène ferrique. La composition de ce dernier, *ca.*  $Wo_{20}En_{15}Fs_{65}$ , le plagioclase aciculaire ( $An_{35-55}$ ,  $\leq 2.5\%$  FeO), les globules à Fe–Ti–P, et le verre intergranulaire de la mésostase, sont conformes avec l'hypothèse d'un bain fondu interstitiel évoluant dans un milieu en déséquilibre, compte tenu du refroidissement rapide des coulées. Les caractéristiques minéralogiques et chimiques sont celles dues à une immiscibilité dans un liquide résiduel d'un système basaltique. La présence dans cette suite (1) d'une pegmatite mafique à clinopyroxène ferrique, (2) de minces liserés

<sup>§</sup> E-mail address: kontaktj@gov.ns.ca

(1–2 cm) de rhyolite associés aux pegmatites mafiques, et (3) de pipes de ségrégation localement abondantes de compositions mafique–felsique mixtes, résulterait de la mobilisation des liquides immiscibles, l'un riche en fer, l'autre riche en silice.

(Traduit par la Rédaction)

*Mots-clés:* basaltes de North Mountain, tholéiites, immiscibilité, Baie de Fundy, Nouvelle-Ecosse.

## INTRODUCTION

The present study focuses on the late-stage crystallization history of the Jurassic (201 Ma; Hodych & Dunning 1992) North Mountain Basalt (NMB) of the Fundy Basin of southern Nova Scotia, a sequence generally known for its abundant and varied zeolites (Colwell 1980, Pe-Piper 2001). Within these quartz-normative continental tholeiites, petrological evidence, both textural and chemical in nature, suggests that liquid–liquid unmixing occurred late in the crystallization history of the basaltic rocks. In addition, vesicle or segregation pipes (also called diktytaxitic pipes; Anderson *et al.* 1984, Goff 1996), mafic pegmatites, and rhyolite bands (Greenough & Dostal 1992a, b, DeWolfe *et al.* 2001) in the NMB are considered to be products of the same immiscibility process (Kontak & Dostal 2002). Herein we document that immiscible Fe–Ti–P- and Si-rich liquids conforming to those compositions predicted by Philpotts (1982) to occur within quartz-normative continental tholeiites are well preserved within the NMB. Although this is not the first petrological study of the NMB (*e.g.*, Mallinson 1986, Papezik *et al.* 1988, Greenough *et al.* 1989, Greenough & Dostal 1992a, b, c), it is the first detailed petrographic study focusing on the nature of the matrix material, in particular the mesostasis within which the textural and chemical evidence of immiscibility occurs.

## GEOLOGICAL SETTING AND NATURE OF THE NORTH MOUNTAIN BASALT

The North Mountain Basalt (NMB) crops out as a thick (300 to 470 m; Stevens 1980, Mallinson 1986, Papezik *et al.* 1988) sequence of basaltic flows forming a northeast- to southwest-trending cuesta of approximately 200 km along the southeastern margin of the Fundy Basin of Maritime Canada in southern Nova Scotia (Fig. 1). Lesser amounts of correlative rocks occur along the northern margin of this basin and also as islands within the Bay of Fundy (*e.g.*, Isle Haute, Grand Manan; Greenough *et al.* 1989). The NMB constitutes the northernmost extent of a large igneous province or LIP, formally referred to as the Eastern North America LIP. Detailed stratigraphic, paleontological, geochronological and geophysical work within the correlative Newark Basin indicates that eruption occurred at 200 Ma and terminated within 0.5 Ma. The extent of this LIP, related to the opening of the central Atlantic Ocean, is impressive. It has recently been extended to cover

parts of western Europe, Africa and South America on the basis of similarities in geochronology and magma composition (summary in Marzoli *et al.* 1999) and is now referred to as the Central Atlantic Igneous Province (CAMP). The estimated original extent of CAMP volcanism is  $4.5 \times 10^6$  km<sup>2</sup>. Given the similar nature of these continental tholeiites, it is, therefore, important to note that features documented within the NMB may well exist within the entire CAMP basalts.

The NMB flows overlie red, fluvial-lacustrine sediments of the Upper Triassic to Lower Jurassic Blomidon Formation, and are overlain by red, fluvial-lacustrine sediments of the Jurassic Scots Bay and McCoy Brook formations. The stratigraphic framework and setting of these bounding sedimentary formations are well documented (Olsen 1988, Olsen *et al.* 1987), hence, so is the general setting at the time of eruption of the subaerial tholeiites of the NMB. Between these sedimentary formations, the intervening NMB flows are subdivided into three broad members, informally referred to as lower, middle, and upper, based on the nature and thickness of the flows (Stevens 1980, Mallinson 1986, Papezik *et al.* 1988, Greenough *et al.* 1989, our studies).

The lower member is a single massive flow interpreted to have been ponded with a maximum thickness of 185 m in the Digby area (Lollis 1959, Papezik *et al.* 1988). This flow, nearly continuously exposed in the field and observed in drill core, is characterized by its homogeneous texture, color, and structure. The flow is dark grey-green, and has well-developed columnar jointing (<1–2 m) and local entablature structure. Bands (several 10s of cm thick) of mafic pegmatite occur in the upper part of this unit near Digby and McKay Head (Fig. 1; Lollis 1959, Greenough & Dostal 1992a, b). The top of the lower flow is marked by a 2- to 3-m-thick amygdaloidal zone.

The overlying middle member consists of several ( $\leq 14$ ) thin (*i.e.*,  $\leq 14$  m) flows, which may be continuous over several km and have features typical of pahoehoe flows. The flows are chilled at the top and bottom (4- to 6-cm-thick zones) and are vesicular. The following zonations typical of continental tholeiites (*e.g.*, Aubele *et al.* 1988) occur in the middle member of the NMB (Kontak 2000): (i) basal pipe vesicles, (ii) intermediate vesicle cylinders, (iii) a net-textured zone, and (iv) a frothy top. The vesicles have been filled with a variety of zeolites, whose nature and origin have recently been discussed in detail by Pe-Piper (2001). The textures of the middle flows are variable owing to their relative thinness and highly vesiculated nature. Fresh

samples have a dark grey-green to black color, a low phenocryst content, are generally fine-grained, and have a considerable proportion of glass (30–40%), which contrasts with the lower and upper members.

The upper member, with a maximum thickness of 154 m (Lollis 1959) in the western end of the exposed NMB, is best sampled on Long Island (Lollis 1959, Mallinson 1986, our studies). In most places, this member consists of a single massive and columnar-jointed flow, with the entablature restricted to the lower part (Mallinson 1986), but in some places (*e.g.*, Freeport), there are clear breaks in the colonnade pattern, suggesting that more than one flow may be present (our studies). In outcrop, the basalt is dark grey-green, contains  $\leq 30\%$  dark green to black irregular blebs and has a variable content of phenocrysts ( $\leq 30\%$ ).

The age of the NMB is constrained by a U/Pb zircon age of  $202 \pm 1$  Ma (Hodych & Dunning 1992) for a pegmatite sampled from the lower member near Digby. A whole-rock  $^{40}\text{Ar}/^{39}\text{Ar}$  age of  $201 \pm 2$  Ma, also for a sample from the basal flow near Digby (unpubl. data of Kontak), is concordant with the zircon age, indicating, therefore, rapid crystallization and cooling of the basalt to below  $300^\circ\text{C}$  (McDougall & Harrison 1988). A similar conclusion is inferred from paleontological evidence, suggesting that the NMB formed in less than 580,000 years (Olsen *et al.* 1998).

#### PETROGRAPHY OF THE NORTH MOUNTAIN BASALT

The petrographic features of the NMB strongly correlate with stratigraphic position of the samples and the

degree of crystallization within the flows. The lower and upper flows are similar, with the exceptions noted below. These basalt flows are dominantly holocrystalline with subhedral to euhedral clinopyroxene and plagioclase (Fig. 2a), subhedral to anhedral opaque grains, and rare orthopyroxene. Rarely, both plagioclase and clinopyroxene may contain melt inclusions, either zonally arranged or along healed fracture-planes. Plagioclase shows normal and oscillatory zoning with an absence of corrosion features or sieve textures. As the character of the opaque phase is relevant to the origin of liquid immiscibility (Philpotts 1982), we note in particular the coarse grain-size of this phase, its absence as inclusions in the silicate phases, and its subhedral to anhedral shape. Although the lower and upper flows are massive and mostly nonvesicular, the upper flow contains the following features not present in the lower flow: (1) mesostasis (30%, Figs. 2b, c) with various textures (see below), including interstitial glass, and (2) a late-stage glass (Fig. 2d) or granophyre with an acicular apatite-group mineral.

The middle flow units contrast markedly with the lower and upper flows in two ways, the texture of the crystallized phases and the abundance and nature of the mesostasis. With respect to the crystallized phases, they vary from coarse to fine grained, equant to trachytic; there is a variable amount of phenocrystic phases, with rare glomerocrysts of plagioclase–pyroxene. These aforementioned features can generally be related to position within the thin flows, with coarser features within the interior. We list here variable features of the mesostasis, accounting for  $\leq 50\%$  of the volcanic

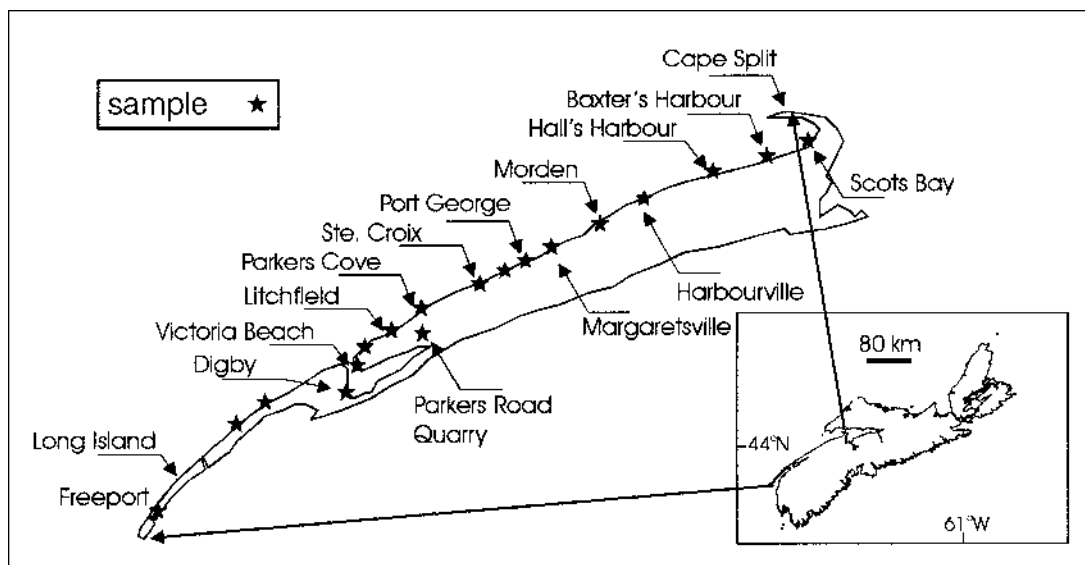
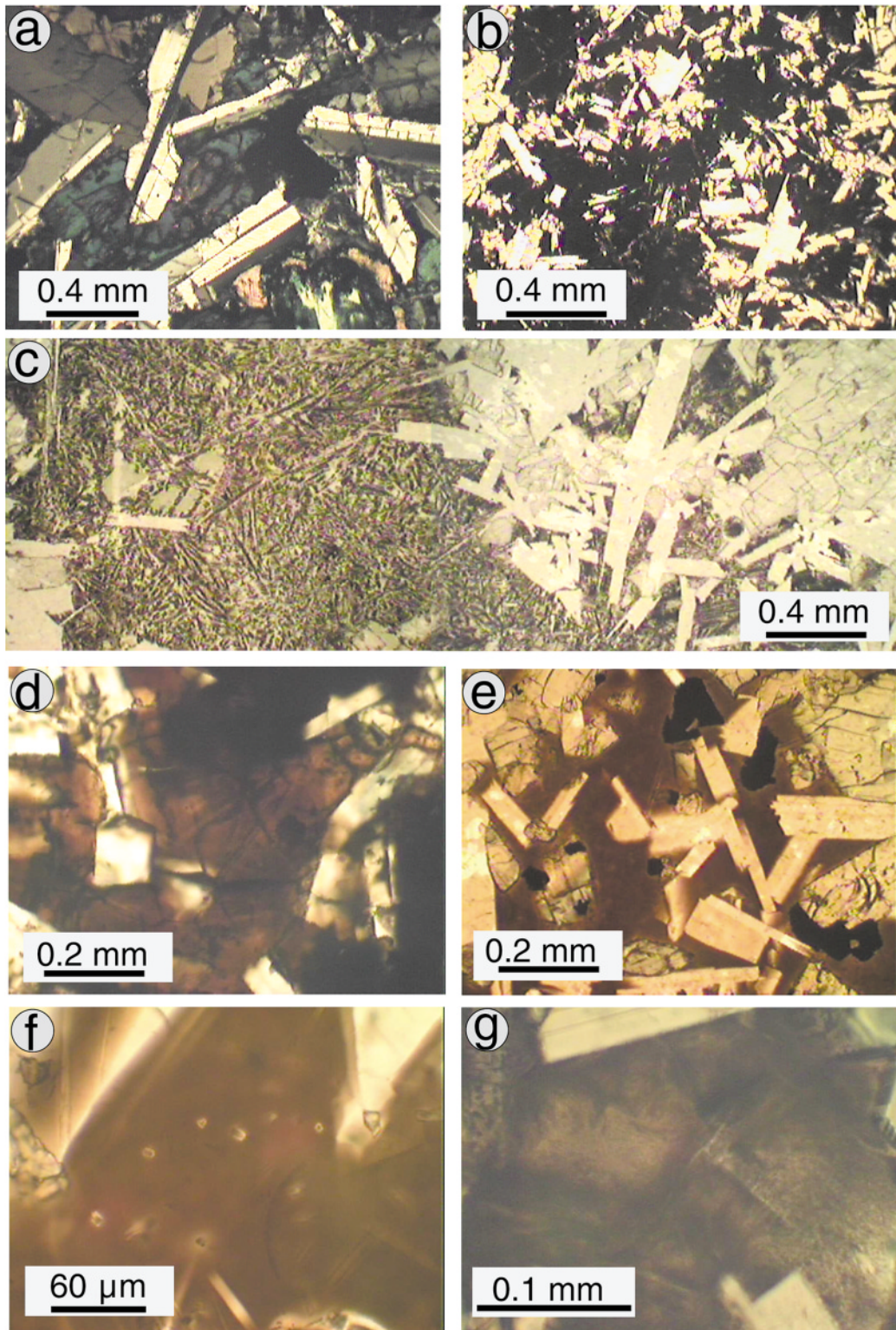


FIG. 1. Location of the North Mountain Basalt Formation in southern Nova Scotia, showing sample sites used in this study, along with geographic points referred to in the text.



samples and representing a late-stage residual melt. (1) There is a dark brown to nearly opaque material in which the silicate minerals and textures are not discernable in transmitted light (Fig. 2b), but within which abundant skeletal oxide is observed in reflected light. Rare, irregularly shaped blebs of altered quenched residual glass occur, now a greenish material (Figs. 3j, k, l). (2) There is variably crystallized, dark red-brown material with skeletal phases of oxides and clinopyroxene (confirmed by EMPA, see below), and elongate microlites of plagioclase are hosted by a residual glass of dark brown, green, or red-brown color. The range in textures of this type of mesostasis, clearly the most common in the flows, is summarized in Figure 3 (a to e). In addition, the percentage of glass interstitial to the skeletal phases and its texture in this mesostasis vary considerably. (3) Uniform red-brown (Figs. 2e, f) and green (Fig. 2g) glass are rare, but where present, it generally amounts to 10–30%. The outline of the glass is defined by the bounding euhedra of plagioclase and pyroxene grains. Rare inclusions of skeletal “apatite” occur within the glass. Notably, there is no oxide phase in the glass. These aforementioned textural features are important, as they clearly indicate that this material represents a melt. In addition, the rim of the glass phase is in some cases outlined by a thin layer of quartz.

FIG. 2. Photomicrographs of North Mountain Basalt samples (see Fig. 1 for locations). Plane-polarized light except in Figure 2a, which is taken in crossed nicols. (a) Holocrystalline basalt from the lower flow unit, sampled at the Parker Road quarry, showing typical coarse-grained basalt with a plagioclase–clinopyroxene intergrowth. Note the complete absence of mesostasis material and the coarse, euhedral grain of an opaque phase in the middle of the photo. The glomeroclasts in flow units 2 and 3 have a similar texture. (b) Mesostasis-rich (*i.e.*, 25–30%) basalt typical of the middle and upper flow units. The dark mesostasis contains abundant, fine-grained disseminated skeletal opaque phases whose opacity inhibits viewing of the finer-grained silicate phases and glass of the mesostasis. Sample of middle flow unit at Baxter’s Harbour. (c) Composite photomicrograph illustrating the coarse holocrystalline part of basalt and the quenched mesostasis surrounding it. The mesostasis contains abundant skeletal pyroxene, minor acicular plagioclase and interstitial glass (now devitrified). Sample of upper flow unit from Parker Cove. (d) Close-up of red-brown glass (57 wt.% SiO<sub>2</sub>) in matrix of basalt from upper flow unit. Sample from Parker Cove area, but about 1 km from previous sample. (e) Basalt with abundant, homogeneous, red-brown felsic glass (74 wt.% SiO<sub>2</sub>). Sample from middle flow unit north of Scots Bay area. (f) Close-up of glass in Figure 2e showing small, disseminated crystallites of apatite. These grains have a skeletal habit in BSE imaging (Fig. 4j). (g) Close-up of greenish felsic glass (70 wt.% SiO<sub>2</sub>), now finely crystalline owing to devitrification (see BSE image in Fig. 4k). Sample from middle flow unit in area northeast of Scots Bay.

The mesostasis of the middle flow units, of irregular shape and filling interstitial space in partially crystallized basalt (Fig. 3a), is texturally the most variable feature within the NMB. In plane light, we note the following features. (1) Flamboyant, skeletal textures are defined by either clinopyroxene or plagioclase (Fig. 3b, j). (2) Skeletal to dendritic opaque phases have a highly variable grain-size and abundance (Figs. 3c, d, e). The abundance of the opaque phases is one of the best indicators of the variable Fe content of the residual liquid (Philpotts 1982). (3) There are variable amounts of interstitial glass (Figs. 3d, e, f). (4) Areas of homogeneous, pale green material (Figs. 3j, k, l) occur in a variety of settings and are inferred to represent late felsic liquid (see details of EMPA below). (5) The presence of small ( $\leq 10\text{--}20\ \mu\text{m}$ ) spheres (Figs. 3g, h, i), referred to herein as globules, that are characterized by variable reflectivity owing to variable amounts of silicate and oxide phases (discussed below). These phases, commonly either attached to or proximal to the skeletal pyroxene or plagioclase, are similar to the immiscible, metal-rich spheres illustrated in Philpotts (1982).

#### SAMPLE SELECTION AND ANALYTICAL TECHNIQUE

Samples of NMB were prepared for standard study of polished section and electron-microprobe analysis. Mineral compositions were established, and a detailed mineralogical study using back-scattered electron and secondary-electron imaging (BSE and SEI, respectively) was done at Dalhousie University, Halifax, Nova Scotia, using a JEOL 733 Superprobe with the following operating conditions: 1–3  $\mu\text{m}$  beam, 15 kV accelerating voltage, 5 nA beam current, and 40 s counting time. Data reduction was carried out with the ZAF software. In addition to point analysis, rastering of mesostasis areas was also done at various scales in order to get bulk compositions using similar procedures, as recently discussed by De Jong & Owen (1999).

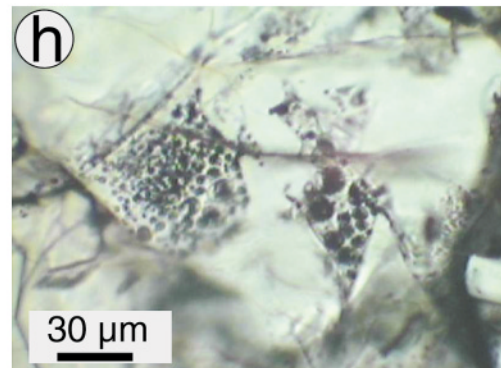
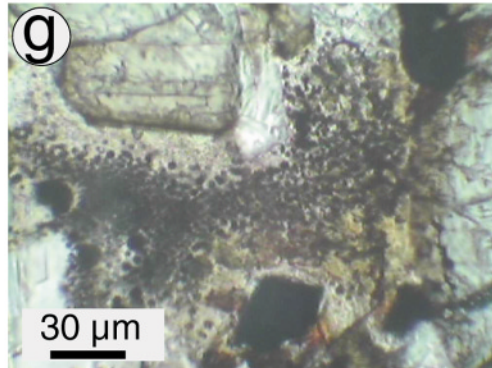
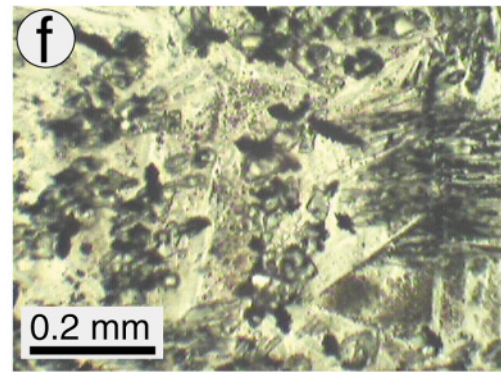
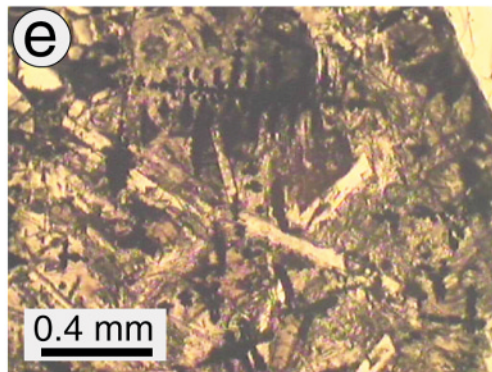
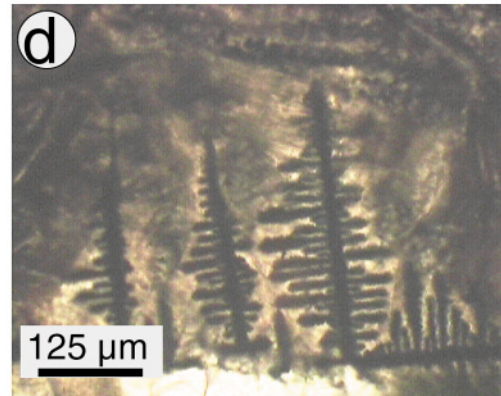
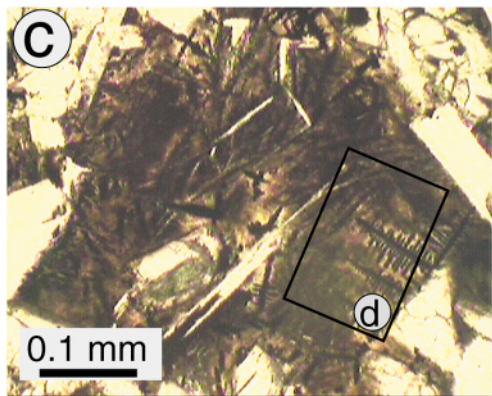
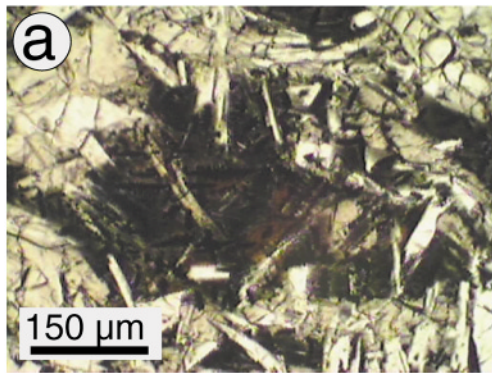
#### ANALYTICAL RESULTS

The features of the samples revealed from image analysis are first summarized. This work was integral to the selection and interpretation of the various chemical data. The chemical composition of phases discussed below refer, respectively, to the coarser-grained part of the samples and to the finer-grained, quenched part, which is interpreted to represent a residual melt (*cf.* Fig. 2c).

#### Image analysis of selected samples

Selected samples were examined using both SEI and BSE facilities on the electron microprobe, and the following observations were noted.

1. The abundant quench-induced textures are dominated by skeletal oxides and clinopyroxene, with less



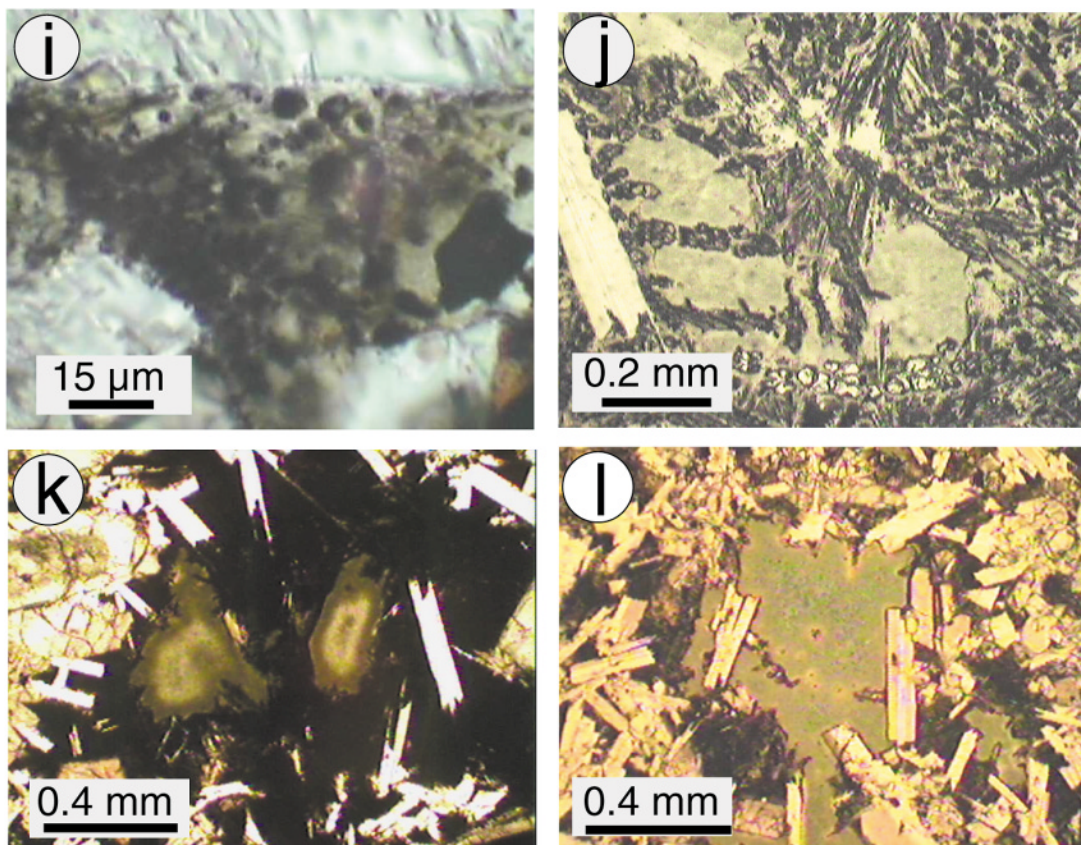


FIG. 3. Photomicrographs showing features of the mesostasis in samples North Mountain Basalt Formation. (a) Typical dark mesostasis consisting of abundant skeletal oxides and intergranular glass. The abundant oxide phases make the mesostasis nearly opaque. (b) Mesostasis rich in skeletal clinopyroxene (cpx), minor skeletal oxide, and intergranular glass. (c, d) Dark mesostasis rich in skeletal oxide phase and dark brown glass. Close-up of typical skeletal oxide is shown in Figure 3d. (e) Mesostasis with abundant fine-grained Fe-rich clinopyroxene and coarser skeletal oxide and acicular plagioclase. (f) Mesostasis with abundant fine-grained, equant, Fe-rich clinopyroxene and plagioclase with intergranular glass. Note triangular area in lower right contains abundant globular phases under higher magnification. (g) Intergranular glass with abundant globules surrounding plagioclase grains. (h) Globules inside plagioclase grain. This occurrence is similar to that described by Philpotts (1981). (i) Globules in intergranular glass with plagioclase grains surrounding the mesostasis. (j) Mesostasis containing skeletal, Fe-rich clinopyroxene and an altered, intergranular, greenish glass. (k) Dark mesostasis cored by greenish material inferred to represent altered residual glass. (l) Plagioclase-rich mesostasis with late-stage glass, now an altered greenish phase.

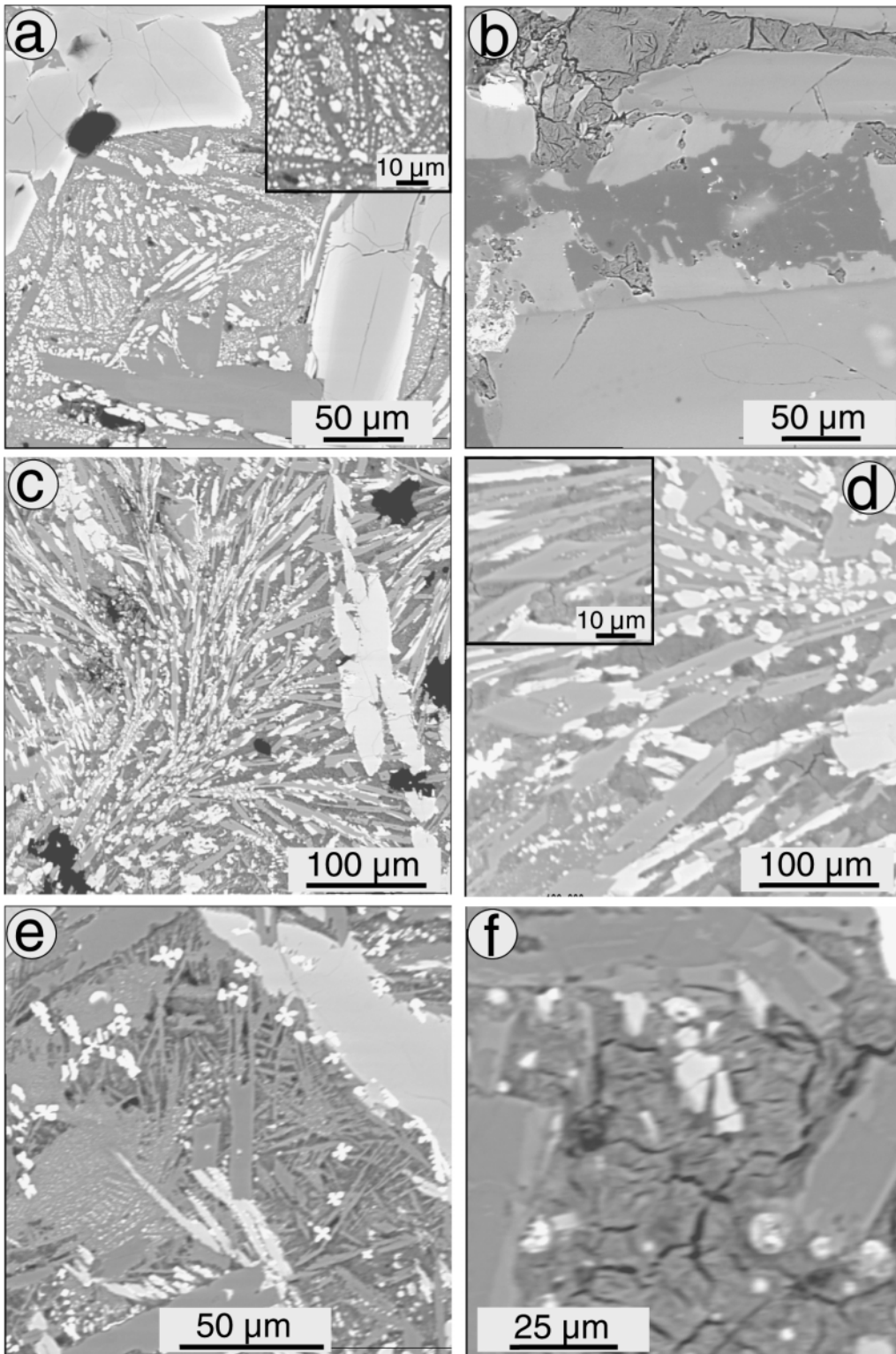
common acicular plagioclase (Figs. 4a, c, d, e). The intervening material is either glass, altered glass (Figs. 4d, f) or variably crystallized material, including an intergrowth of quartz and feldspar (Fig. 4b) and fine-grained crystallized material not resolvable with the electron microprobe (Fig. 4k).

2. A narrow, Fe-rich overgrowth of clinopyroxene covers earlier, Mg-rich clinopyroxene where it is in contact with the mesostasis (Fig. 4a).

3. A sodic overgrowth on plagioclase is present where it borders the mesostasis (Fig. 4b). In contrast to

the texture of the pyroxene overgrowth, the sodic feldspar continues into and is intergrown with mesostasis material; consequently, the overgrowth has a ragged texture.

4. The felsic glass, represented by greenish and red-brown material in transmitted light (Fig. 4j), has a homogeneous texture. Rarely, the glass is dominated by a very fine-grained and delicate patterns of fibers ( $\leq 1\text{--}2\ \mu\text{m}$  width, Fig. 4k), producing a hair-like texture. The fine-grained nature of this material precluded a determination of its mineralogical and compositional nature.



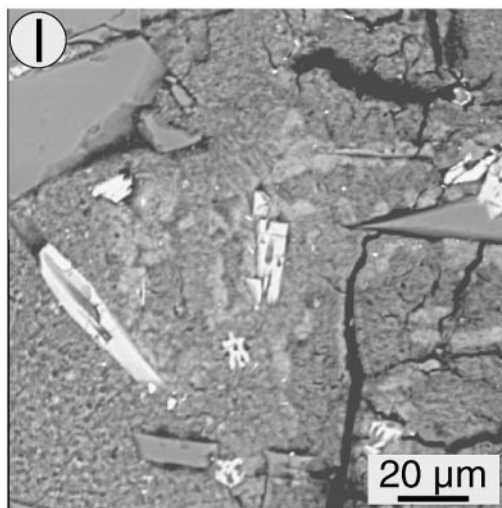
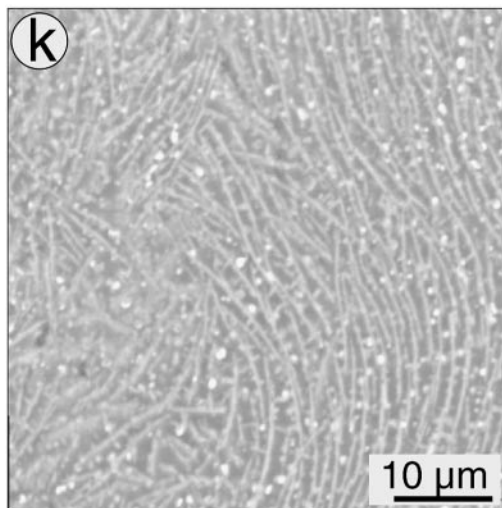
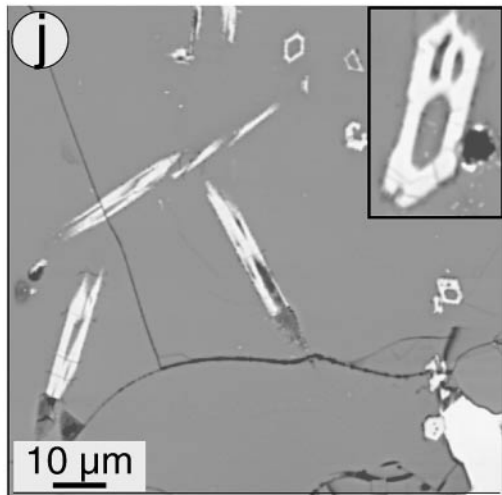
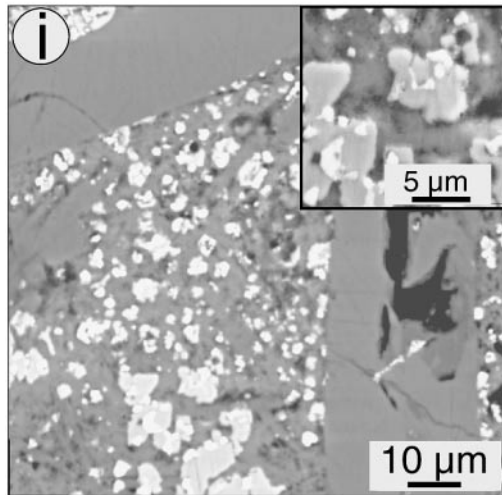
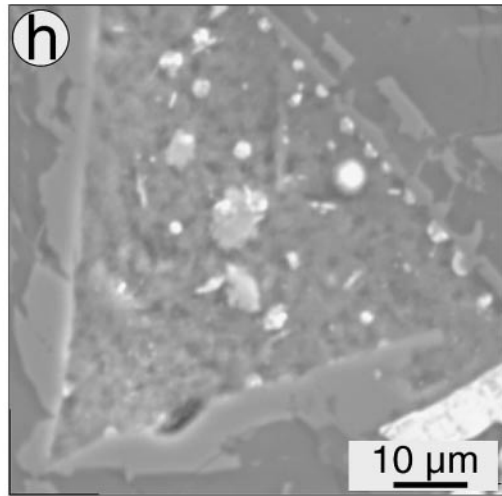
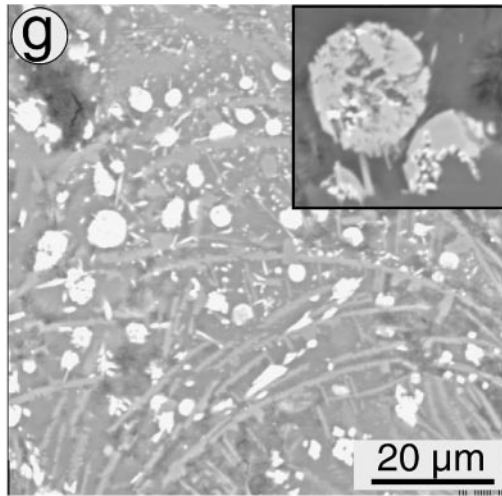


FIG. 4. Back scattered electron (BSE) and secondary electron (SEI) images of North Mountain Basalt samples (all are BSE unless indicated otherwise). (a) Mesostasis surrounded by zoned clinopyroxene (cpx) grains and large plagioclase grain (dark grey in bottom of image). Note the Fe-enrichment on the rim of the clinopyroxene grains where they are in contact with the mesostasis. The mesostasis is dominated by skeletal, Fe-rich clinopyroxene (it is as bright as the rim on cpx phenocrysts), skeletal Fe–Ti oxides, and very small, subrounded globules of Fe–Ti-rich silicate. The inset image shows an enlargement of mesostasis area containing the globules. (b) Calcic plagioclase grain ( $An_{65}$ ) of the matrix with narrow sodic rim or overgrowth ( $An_{8-10}$ ; dark part of grain). The intergranular area between plagioclase consists of alkali feldspar ( $Or_{80-90}Ab_{10-20}An_{5-10}$ ) that envelops an area of quartz (uniform dark grey). Note the medium grey material with a crack texture along the top of the photo; it is an altered, devitrified glass. (c) Mesostasis with flamboyant-textured calcic plagioclase (grey phase), rare coarse clinopyroxene (bright phase on right), and small skeletal Fe-rich clinopyroxene. In detail, there are abundant subrounded globules decorating faces of the acicular plagioclase grains. Material between the plagioclase and clinopyroxene is glass. (d) Acicular and skeletal plagioclase in mesostasis with Fe-rich clinopyroxene in a devitrified glass (dark grey intergranular material with crack texture in lower right). Inset image shows skeletal plagioclase grains 20  $\mu\text{m}$  long that form chains. (e) Combined BSE and SEI image illustrating texture and composition of quenched mesostasis. Large grain of clinopyroxene on right has skeletal oxides decorating margin. Note the two sizes and shapes of plagioclase grains (*i.e.*, equant and acicular types). The intergranular material is a quenched glass. (f) Combined BSE and SEI image showing the nature of the devitrified mesostasis glass with desiccation (?) cracks. Present in lower right are some small globular phases that have unmixed (see text for discussion). (g) Quenched mesostasis with acicular, flamboyant plagioclase grains and Fe–Ti–P-rich globules hosted by intergranular glass. Inset image shows enlargement of unmixed globule 10  $\mu\text{m}$  wide, with silicate- and Fe–Ti–P-rich parts. (h) BSE and SEI image of intergranular mesostasis between plagioclase grains showing variation in composition of the globule phase. (i) Mesostasis enriched in globules that have unmixed during subsolidus re-equilibration to silicate- and Fe–Ti–P-rich phases. Inset figure shows the pyroxene-like phase formed from the globules with the equant shape that they have now assumed. (j) Felsic (*i.e.*, 74 wt.%  $\text{SiO}_2$ ) glass in matrix of basalt that is decorated with skeletal crystals of “apatite” (inset is enlargement of a grain 15  $\mu\text{m}$  long). Note the homogeneous composition of the glass indicated by the BSE image and confirmed by point analysis. (k) Felsic glass of similar composition to that in Figure 5j, but with devitrification or quench texture. The thin fibers define a hair-like texture; the grain size precludes resolving the mineralogy and compositions, but the fibers seem to have a feldspar composition. Note the presence of the Fe–Ti-rich globular phase disseminated throughout. (l) Altered intergranular glass of probable felsic composition. Note the presence of the skeletal Fe-rich clinopyroxene (coarser rectangular grains) and “apatite” (smaller grains), whose presence is important when inferring the origin and nature of this mesostasis.

Disseminated within some of the felsic glass are skeletal “apatite” and a pyroxene (Figs. 4j, l). Some of the felsic glass is altered to an unresolved intergrowth of fine-grained phases (Fig. 4l).

5. A phase with negative relief in SEI is considered to be a residual melt (Fig. 4h), now altered to an undetermined secondary phase (discussed below). This material commonly displays a regular pattern of cracks that possibly relate to dehydration (Figs. 4f, l).

6. Disseminated spheres of mixed silicate–oxide character (Figs. 4a, f, g, h) are highly variable in texture and composition but, in general, tend to assume the morphology of pyroxene crystals where dominated by a silicate composition (*i.e.*, Fe-rich pyroxene; Figs. 4h, i), and a spherical morphology where of oxide composition (Figs. 4a, h). The spheres tend to occur in clusters and are preferentially attached to plagioclase grains, a feature also noted by Philpotts (1982). The spheres are also present within the felsic glass characterized by the fine-grained fiber texture (Fig. 4k).

#### Composition of the matrix

The host to the mesostasis-rich middle flow units is zeolite-bearing basalt; therefore, whole-rock compositions of such material are suspect because of potential elemental gains and losses associated with zeolite for-

mation (Pe-Piper *et al.* 1992, Kontak 2000, unpubl. data). In order to estimate the primary composition of the middle flow units of the NMB, raster analyses of matrix material collected away from both mesostasis and zeolite-occluded amygdules were obtained. The compositions are comparable to whole-rock data for fresh NMB (Fig. 5a); representative results are given in Table 1. The matrix compositions define a tight cluster except for three cases that tend toward the silica apex of the diagram, probably reflecting a felsic component in the matrix (see below). The results of the raster and whole-rock analyses generally overlap, although there is a clear trend of the matrix data away from the whole-rock data, indicating *in situ* fractionation on the micro-scale. This fractionation trend is also suggested by other data to be discussed below.

#### Composition of mesostasis

Two distinct types of mesostases (herein distinguished from the matrix as being finer-grained and representing the residual melt that last crystallized) were analyzed, the more abundant being a quenched, residual basaltic melt (*e.g.*, Figs. 2b, c) and a less abundant intergranular melt (Figs. 2e, f, 4c, j). In addition, both raster and point (10–40  $\mu\text{m}$ ) analyses were made, and the data are summarized in a triangular plot in Figure 5, with

representative compositions given in Table 1. We note that there is an overlap of the mesostasis composition with the matrix data (Figs. 5b, c), albeit with greater variation and more data trending toward silica-rich compositions. In general, there is a large range of compositions, reflecting variations in the dominant mineral components, namely plagioclase, pyroxene, alkali feldspar and quartz, which relate to variable degrees of crystallization of the liquids. In the triangular plots, there is a distinct progression of the data toward the silica apex of the diagram, which reflects the development within the mesostasis of a silica-rich glass (*i.e.*, 75 wt.% SiO<sub>2</sub>).

Other important aspects of these data are summarized as follows: (1) The range in silica (mostly 48–75 wt.% SiO<sub>2</sub>) spans basaltic to rhyolitic compositions. Many of these data points pertain to a uniform intergranular phase interpreted to represent quenched glass. The large variation in the compositions of this residual glass reflects variable amount of *in situ* fractionation that occurred prior to quenching. (2) There is a group of data points specifically related to the greenish areas of irregular to regular shape (Fig. 2l, Table 1, anal. ZL-99-06b), with enrichment of K (*i.e.*, 10 wt.% K<sub>2</sub>O). This type of mesostasis is considered to represent hydrolytically al-

TABLE 1. REPRESENTATIVE COMPOSITIONS OF MATRIX, MESOSTASIS, AND GLASS IN SAMPLES OF NORTH MOUNTAIN BASALT, NOVA SCOTIA

Sample	Comments	SiO <sub>2</sub>	TiO <sub>2</sub>	Al <sub>2</sub> O <sub>3</sub>	FeO	MnO	MgO	CaO	Na <sub>2</sub> O	K <sub>2</sub> O	P <sub>2</sub> O <sub>5</sub>	BaO
<b>Matrix</b>												
ZL-99-02A		56.35	0.97	15.77	8.22	BD	4.31	9.07	3.71	1.20	BD	0.40
ZL-99-02A		56.94	1.28	13.94	9.49	BD	5.31	8.60	2.63	1.64	BD	0.17
ZL-99-01A		55.42	1.79	12.47	13.46	BD	4.38	5.41	6.88	0.19	BD	0.00
ZL-99-01A		57.13	1.33	12.92	11.14	BD	4.60	5.16	7.33	0.29	BD	0.10
ZL-99-06A		55.94	1.86	12.50	11.56	0.20	4.72	4.90	7.04	0.96	0.31	BD
ZL-99-09a		53.87	1.09	14.91	9.50	0.25	6.68	8.57	3.88	1.19	0.05	BD
<b>Mesostasis rastered</b>												
ZL-99-5	quenched	59.66	0.37	17.41	9.85	BD	6.65	1.32	0.54	3.77	0.29	0.13
ZL-99-5	quenched	59.14	0.46	19.49	6.90	BD	1.30	3.99	7.62	0.69	0.36	0.04
ZL-99-5	quenched	56.15	1.63	17.78	8.95	BD	0.54	5.96	7.47	0.36	0.98	0.12
ZL-99-06b	brown mesostas.s	60.87	0.80	18.82	4.61	BD	2.90	4.03	6.97	0.88	BD	0.11
ZL-99-06b	brown mesostas.s	62.24	0.91	15.65	5.20	BD	2.92	0.96	2.76	8.99	BD	0.35
ZL-99-06b	altered green glass	59.63	0.14	4.92	16.17	BD	7.93	0.22	0.82	10.17	BD	BD
ZL-99-06b	altered green glass	57.94	BD	5.58	18.61	BD	6.42	0.98	1.04	9.25	BD	BD
ZL-99-06b	altered green glass	59.30	BD	1.67	21.38	BD	7.19	0.13	0.17	10.11	BD	BD
z-99-27	quenched	53.17	2.19	15.01	12.40	0.17	4.26	7.57	3.68	0.76	0.58	0.22
z-99-27	quenched	57.93	2.55	12.33	11.93	0.22	2.82	7.37	3.76	0.62	0.47	BD
ZL-99-38	quenched	60.82	0.44	19.11	5.94	BD	1.83	4.79	4.94	1.29	0.56	0.25
ZL-99-38	quenched	56.72	4.43	15.63	7.69	BD	3.03	4.50	3.72	3.61	0.66	BD
<b>Glass in mesostasis</b>												
ZL-99-27	altered, dark brown	58.85	0.12	25.28	0.98	BD	BD	8.48	5.62	0.61	BD	BD
ZL-99-27	altered glass, dark brown	61.50	0.36	8.45	10.08	BD	9.27	0.25	0.30	9.80	BD	BD
ZL-99-20a	homogeneous red-brown	75.86	0.80	11.86	3.87	1.53	BD	4.39	1.68	BD	BD	BD
ZL-99-20a	homogeneous red-brown	76.08	0.61	11.63	4.15	1.54	BD	4.36	1.64	BD	BD	BD
ZL-99-20c	devitrified glass	72.66	0.44	15.91	2.29	BD	0.29	4.75	2.67	0.62	0.38	BD
ZL-99-20c	devitrified glass	74.68	0.37	15.33	1.48	BD	0.20	3.95	2.99	0.76	0.23	BD
ZL-99-38	intergranular material	75.71	0.17	13.35	1.21	BD	0.17	2.94	4.79	0.69	0.72	0.16
MD8-7		59.20	0.43	20.09	4.52	BD	2.50	6.40	5.03	1.33	0.47	BD
MD8-8		61.47	0.36	22.77	1.49	BD	0.13	8.02	5.05	0.55	0.16	BD
NMB-08	red brown glass	57.08	BD	6.74	8.56	BD	24.67	2.28	0.67	BD	BD	BD
ZL-99-5	intergranular glass	55.20	1.34	17.57	8.60	0.11	4.54	4.76	2.62	3.32	1.81	0.12
ZL-99-6A	intergranular glass	51.23	2.31	14.34	16.13	0.44	0.93	3.69	7.73	1.63	1.43	0.13
ZL-99-6A	intergranular glass	58.42	0.38	13.79	9.67	0.17	1.97	2.94	4.20	7.51	0.95	BD
ZL-99-06	darker area in image	61.95	0.23	15.95	8.37	BD	0.76	3.01	4.92	3.22	0.87	0.72
ZL-99-06	lighter area in image	64.35	0.15	17.97	3.52	BD	0.37	1.20	8.01	4.07	BD	0.35
ZL-99-09b	altered glass	57.62	BD	11.63	9.75	BD	11.34	1.05	0.29	8.32	BD	BD
ZL-99-09b	altered glass	59.13	BD	11.57	9.99	BD	11.13	0.80	BD	7.38	BD	BD
NMB-08	dk red brown	50.94	BD	7.63	19.20	BD	18.01	3.57	0.65	BD	BD	BD
NMB-08	dk red brown	57.08	BD	6.74	8.56	BD	24.67	2.28	0.67	BD	BD	BD

Results of analyses are normalized to 100 wt.%; BD: below detection limit.

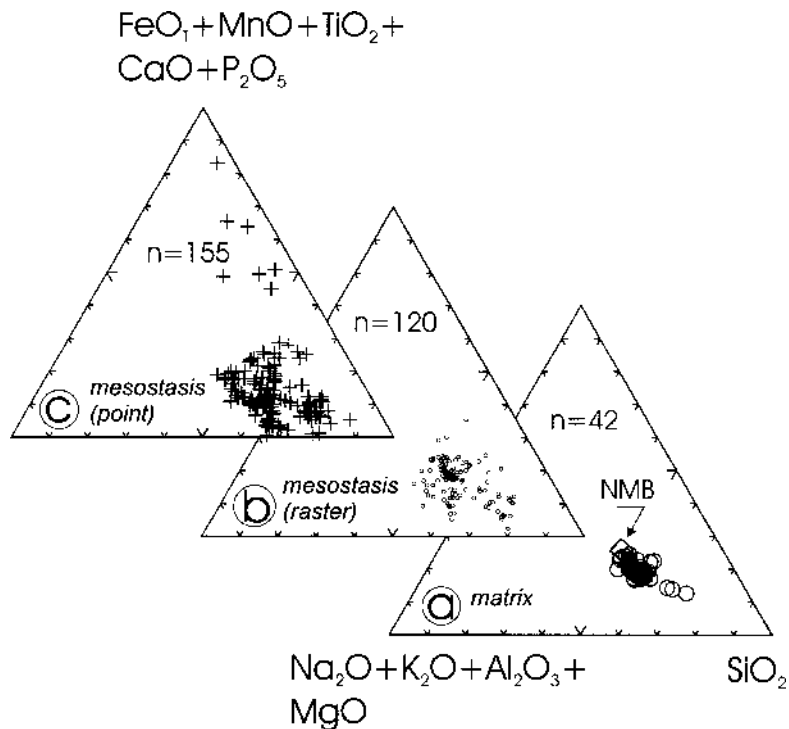


FIG. 5. Plot of chemical data on samples of North Mountain basalt in terms of the  $(\text{FeO} + \text{MnO} + \text{TiO}_2 + \text{CaO} + \text{P}_2\text{O}_5) - (\text{Na}_2\text{O} + \text{K}_2\text{O} + \text{Al}_2\text{O}_3 + \text{MgO}) - \text{SiO}_2$  diagram used by Philpotts (1982). (a) Raster analyses ( $n = 42$ ) of the matrix of NMB compared to whole-rock compositions of NMB (represented by the diamond symbol) compiled from the literature (Wark & Clarke 1980, Dostal & Dupuy 1984, Papezik *et al.* 1988, Greenough & Papezik 1987, Greenough *et al.* 1989, Greenough & Dostal 1992c, Pe-Piper *et al.* 1992). (b) Raster analyses of mesostasis ( $n = 120$ ). (c) Point analyses (10 to 40  $\mu\text{m}$  beam) of the mesostasis ( $n = 155$ ).

tered felsic glass, now dominated by fine-grained mica. (3) Apparently uniform glass (anal. ZL-99-20a, 20c), as observed from petrographic and BSE imaging, can be chemically variable among samples, such that a mesostasis with *ca.* 70–78 wt.%  $\text{SiO}_2$  and 10–15 wt.%  $\text{Al}_2\text{O}_3$  is also enriched in K (~5–7 wt.%  $\text{K}_2\text{O}$ ), Na ( $\leq 3$ –5 wt.%  $\text{Na}_2\text{O}$ ), Ca ( $\leq 3$ –6 wt.%  $\text{CaO}$ ) or Fe ( $\leq 6$ –8 wt.%  $\text{FeO}$ ). (4) There is variable enrichment in phosphorus, with the data extending up to 3.5 wt.%  $\text{P}_2\text{O}_5$ , without obvious trend with respect to silica. (5) The compositions of the mesostasis are similar to liquids that show immiscibility elsewhere, and their compositions are appropriate for the products of such a process.

#### Compositions of the minerals

The mineral phases analyzed include phenocrystic and matrix phases. The phases are discussed together, but because of their petrogenetic importance, the mineral data are plotted separately. Pyroxene compositions

(Table 2) are plotted in the pyroxene quadrilateral, where they are compared to the field for pyroxene from NMB and the Skaergaard crystallization trend (Fig. 6). The coarse pyroxene phases, occurring as phenocryst and matrix grains, correspond to augite and pigeonite with a distinct Fe-enrichment from core to rim that is commensurate with an enrichment in titanium (to 3 wt.%  $\text{TiO}_2$ ; Fig. 7c). The most magnesian (*i.e.*, primitive) composition of these pyroxenes is  $\text{En}_{52}\text{Wo}_{37}\text{Fs}_{11}$ , whereas the most evolved composition is  $\text{En}_{15}\text{Wo}_{35}\text{Fs}_{50}$ . The chemical evolution of the augite is matched by a similar, parallel trend for pigeonite (Figs. 6, 7a, b). The most Fe-enriched pyroxene in the matrix occurs in contact with mesostasis material (Fig. 4a). The mesostasis pyroxene, dominated by skeletal augite with rare pigeonite, shows a chemical evolution similar to that of the coarser pyroxene, but with more extreme enrichment in Fe (*i.e.*,  $\text{En}_8\text{Wo}_{22}\text{Fs}_{70}$ ), Ti, and P (Figs. 6, 7). The enrichment in titanium (to 6 wt.%  $\text{TiO}_2$ ) is not uncommon for terrestrial pyroxene (*e.g.*, Robinson 1980), but the

elevated phosphorus (to 1.6 wt.% P<sub>2</sub>O<sub>5</sub>) is unusual, such that this element is completely excluded from general reviews of pyroxene chemistry (*e.g.*, Robinson 1980). The elevated phosphorus contents occur in mesostasis pyroxene and are correlated with higher Ti contents, but there is no apparent enrichment in Ca, as might be suspected if inclusions of apatite had been encountered. Thus, the origin and nature of the elevated phosphorus in some of the pyroxene remain equivocal. With respect to Mn, there is a consistent trend for all the pyroxenes, both matrix and mesostasis, in the MnO versus FeO binary plot (Fig. 7e).

Plagioclase as a phenocryst and matrix phase shows a distinct zonation from core to rim, An<sub>75-50</sub> and An<sub>70-40</sub>, respectively (Fig. 8, Table 3); the overlap in composition is consistent with the oscillatory zoning observed in these grains. The most sodic compositions occur for matrix plagioclase against mesostasis, where overgrowths are of An<sub>10-2</sub> composition. Plagioclase in mesostasis surrounded by granophyre is unzoned and consistently of An<sub>50</sub> composition, whereas the plagioclase intergrown with granophyre is sodic (An<sub>10</sub>). The mesostasis plagioclase, occurring as microlites of variable texture, ranges from An<sub>48</sub> to An<sub>31</sub> in composition, with slightly more potassium than matrix plagioclase

(Fig. 8). In addition, the mesostasis plagioclase of skeletal habit is characterized by significant amounts of Fe, with a maximum of 2.5 wt.% FeO, in contrast to ≤0.5 wt.% for most plagioclase in NMB. There is a negative correlation between Ca and Fe in such Fe-rich plagioclase.

The nature and composition of the alkali feldspar (Table 3) are as follows: (1) The overgrowth on matrix plagioclase adjacent to mesostasis is Or<sub>70</sub>Ab<sub>30</sub>, (2) the intergranular occurrences are generally Or<sub>62</sub>Ab<sub>38</sub> to Or<sub>75</sub>Ab<sub>25</sub>, but two anomalous compositions of ternary composition occur (*i.e.*, Or<sub>40-50</sub>Ab<sub>50-60</sub>An<sub>10</sub>; Fig. 8), and (3) the granophyre contains Or<sub>80</sub>Ab<sub>20</sub>.

The opaque phase in the NMB is dominantly homogeneous in BSE imaging, but oriented Fe-rich exsolution lamellae do occur within the Fe-Ti oxide host. The range in compositions is summarized in Figure 9, where it is apparent that the homogeneous phase encompasses a large compositional range from *ca.* 45 to 65 wt.% FeO (*i.e.*, ilmenite to ulvöspinel), with more Fe-rich compositions relating to exsolution lamellae. The coarse, equant grains of the matrix are both of ilmenite and ulvöspinel, whereas the skeletal grains are of ulvöspinel composition only. Although dominated by Fe and Ti, the oxide phases do contain minor Al and Mn. The low

TABLE 2. REPRESENTATIVE COMPOSITIONS OF PYROXENE IN SAMPLES OF NORTH MOUNTAIN BASALT, NOVA SCOTIA

Sample	Comments	SiO <sub>2</sub>	TiO <sub>2</sub>	Al <sub>2</sub> O <sub>3</sub>	FeO	MnO	MgO	CaO	Na <sub>2</sub> O	P <sub>2</sub> O <sub>5</sub>	Total	Si	Ti	Al	Fe	Mn	Mg	Ca	Na	P
<b>Coarse pyroxene</b>																				
MD-19a-1	core	52.66	0.56	1.82	7.74	0.21	17.65	19.45	0.30	0.11	100.94	1.926	0.018	0.078	0.240	0.000	0.966	0.762	0.024	0.000
19a-2	rim	51.51	0.82	7.37	9.59	BD	11.85	17.40	1.32	BD	100.42	1.890	0.024	0.318	0.294	0.000	0.648	0.684	0.096	0.000
MD-5a-5	core	53.40	0.25	1.61	7.78	BD	18.79	19.06	0.27	BD	102.16	1.936	0.000	0.066	0.234	0.000	1.020	0.744	0.019	0.000
5a-6	rim	51.28	0.96	1.71	12.75	0.20	14.44	16.63	0.41	0.13	100.71	1.926	0.030	0.078	0.402	0.000	0.810	0.750	0.030	0.000
md8-9	core	54.20	0.17	0.81	15.50	0.28	25.04	4.36	0.21	BD	100.77	1.958	0.000	0.036	0.474	0.006	1.356	0.168	0.016	0.000
md8-10	rim	47.85	1.72	2.87	19.65	0.33	11.79	14.80	0.37	0.15	99.69	1.866	0.048	0.132	0.642	0.012	0.684	0.618	0.030	0.000
md8-24	core	53.42	0.48	0.78	17.52	0.45	22.50	4.61	0.18	BD	100.52	1.982	0.012	0.030	0.540	0.012	1.254	0.192	0.015	0.000
md8-25	rim	47.97	1.61	2.50	19.84	0.48	11.96	14.50	0.25	0.18	99.44	1.878	0.048	0.114	0.648	0.018	0.696	0.606	0.017	0.000
ZL-99-05	core	54.69	0.16	1.2*	12.08	0.18	29.16	2.37	0.22	BD	100.07	1.956	0.000	0.054	0.360	0.000	1.554	0.090	0.016	0.000
ZL-99-06C	core pyx	53.56	0.27	0.78	16.82	0.36	22.76	4.61	0.76	BD	99.79	1.974	0.006	0.036	0.510	0.012	1.254	0.180	0.054	0.000
ZL-99-06C	rim by mesostasis	46.53	1.28	1.39	27.52	0.64	6.02	13.93	0.28	BD	97.67	1.926	0.042	0.066	0.954	0.024	0.372	0.618	0.024	0.000
zl-99-20A	core, glomerocryst	53.37	0.20	0.91	15.60	0.36	26.22	4.64	0.21	BD	100.50	1.950	0.000	0.042	0.474	0.012	1.374	0.180	0.016	0.000
zl-99-20A	rim, glomerocryst	48.79	0.44	0.60	33.00	0.58	10.82	5.14	0.33	BD	99.69	1.962	0.012	0.030	1.174	0.018	0.648	0.222	0.024	0.000
zl-99-12	core	54.67	0.09	0.55	14.42	0.27	26.72	4.21	BD	BD	100.84	1.962	0.000	0.074	0.432	0.006	1.434	0.162	0.000	0.000
zl-99-12	rim	48.76	1.11	1.58	21.56	0.36	10.42	15.85	0.22	0.14	99.66	1.914	0.030	0.072	0.708	0.012	0.612	0.660	0.016	0.000
<b>Matrix pyroxene</b>																				
10a-6	core	44.62	3.00	3.53	26.33	0.41	5.80	15.29	0.24	BD	99.32	1.818	0.090	0.168	0.894	0.012	0.354	0.666	0.018	0.000
ZL-99-01A		54.25	0.20	0.84	13.87	BD	25.31	4.61	0.33	BD	99.41	1.974	0.001	0.036	0.420	0.012	1.374	0.180	0.024	0.000
ZL-99-02A		50.38	0.89	1.22	20.65	BD	11.81	14.75	0.24	BD	99.95	1.944	0.074	0.054	0.666	0.018	0.678	0.612	0.016	0.000
zl-99-09a	rim	44.73	3.39	4.26	32.40	0.49	3.19	9.47	0.85	0.79	99.17	1.824	0.102	0.204	1.104	0.018	0.192	0.414	0.066	0.030
zl-99-09a	core	43.48	3.92	2.12	34.46	0.69	4.03	9.63	BD	1.41	99.17	1.794	0.120	0.102	1.188	0.024	0.246	0.426	0.050	0.048
ZL-99-09b		47.90	0.87	0.95	34.66	0.62	5.71	8.94	BD	BD	99.17	1.968	0.024	0.042	1.188	0.024	0.348	0.396	0.060	0.000
ZL-99-12		47.50	1.79	4.15	18.09	BD	10.82	16.97	BD	BD	99.17	1.848	0.054	0.192	0.588	0.030	0.624	0.708	0.000	0.000
ZL-99-14	rim	47.86	1.99	3.80	23.69	0.34	7.30	14.29	BD	BD	99.17	1.890	0.060	0.180	0.768	0.012	0.432	0.506	0.000	0.000
zl-99-14		45.53	2.71	3.20	26.33	0.51	6.06	15.36	0.41	BD	100.12	1.830	0.084	0.160	0.888	0.018	0.366	0.660	0.030	0.000
zl-99-14		40.86	5.60	3.67	31.31	0.53	4.45	12.81	0.41	0.13	99.84	1.698	0.174	0.180	1.092	0.018	0.278	0.570	0.036	0.000
zl-99-14	core	44.42	2.82	3.99	28.08	0.35	5.94	13.26	0.23	0.11	99.09	1.812	0.084	0.192	0.960	0.012	0.360	0.582	0.017	0.000
zl-99-14	rim	45.04	2.24	3.59	31.40	0.45	5.72	10.86	0.43	BD	99.73	1.836	0.066	0.174	0.974	0.018	0.348	0.474	0.036	0.000
zl-99-025		46.50	1.31	2.64	30.05	0.39	4.97	12.63	0.41	BD	99.17	1.884	0.042	0.126	1.014	0.012	0.300	0.546	0.036	0.000
zl-99-025		47.81	1.34	3.07	27.06	0.45	5.77	13.70	0.44	BD	99.17	1.920	0.042	0.144	0.912	0.018	0.348	0.588	0.036	0.000
zl-99-26		51.93	0.32	1.62	9.34	0.25	17.44	16.70	0.35	BD	99.95	1.926	0.006	0.072	0.288	0.000	0.966	0.744	0.026	0.000
zl-99-26	core	52.04	0.52	1.50	9.70	0.17	18.51	17.15	0.26	BD	99.85	1.926	0.012	0.066	0.300	0.000	1.020	0.678	0.017	0.000
ZL-99-38		41.82	5.12	4.16	33.05	0.62	3.10	9.50	0.61	1.49	99.47	1.722	0.156	0.204	1.140	0.024	0.192	0.420	0.054	0.054
ZL-99-38		40.22	5.77	4.09	35.00	0.56	2.08	8.79	0.93	1.57	99.01	1.686	0.180	0.204	1.230	0.018	0.132	0.396	0.077	0.054

BD: below detection limit. Compositions are quoted in weight %, and in atoms per formula unit.

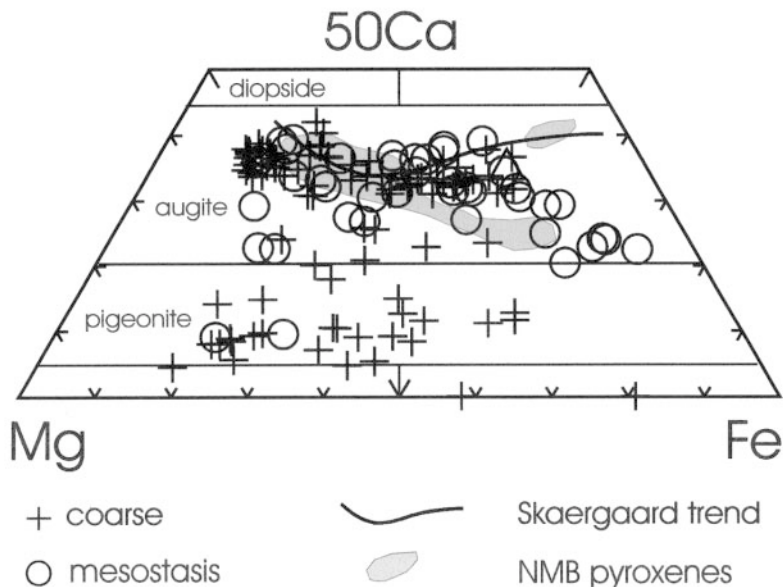


FIG. 6. Pyroxene quadrilateral (50Ca–Mg–Fe) showing compositions of pyroxenes in samples of North Mountain Basalt; pyroxene nomenclature after Morimoto (1989). Coarse refers to pyroxene as phenocrysts or part of the matrix, whereas mesostasis refers to pyroxene within the quenched residual melt part of the basalt now represented by mesostasis. Skaergaard trend from Brown (1957) and Brown & Vincent (1963), and field for NMB pyroxenes from Greenough & Dostal (1992c).

totals (*i.e.*, Fe + Ti) for the skeletal grains relate to interference with the surrounding mesostasis, resulting in dilution of the major-element components of the oxide phase.

The globular phase in the mesostasis (*i.e.*, Fig. 4g) varies from being homogeneous to heterogeneous, with variation in SiO<sub>2</sub>, FeO, CaO, MgO, TiO<sub>2</sub>, and P<sub>2</sub>O<sub>5</sub> (Fig. 10, Table 4). In terms of the nature of the globules, three separate groupings, clearly recognized in BSE imaging (Figs. 4g, h, i), are noted: (1) an Fe-rich pyroxene-like phase of equant shape (Table 5); this phase is plotted separately in Figure 10 where it is compared to a typical composition of a Fe-rich pyroxene in the mesostasis in order to emphasize the pyroxene-like composition of this phase, (2) a silica-rich part of the globules, and (3) an Fe-rich part of the globule and homogeneous Fe-rich globules. Where Fe- and Si-rich phases are together in the same globule, unmixing of an original homogeneous phase seems to have occurred. In terms of composition, there appears to be a continuum among the three groups, but note that some of this may be an artifact of interference during analysis, given the size of the globules. Of particular note with respect to the composition of the globules is the enrichment in phosphorus in the silica-rich phase.

## DISCUSSION

Liquid immiscibility has long been proposed as a significant petrological process in both igneous differentiation and magmatic ore formation. In fact, Philpotts (1982) noted that "...immiscible liquids are present in sufficient amounts in so many volcanic rocks that immiscibility should be considered a viable means of differentiation during late stages of fractionation of common magmas". The role of liquid immiscibility is considered relevant in the formation of a variety of igneous rock-types, including ocean-floor plagiogranites (Dixon & Rutherford 1979), alkaline suites (Philpotts & Hodgson 1968, Eby 1979, 1980, Freestone 1978, Kendrick & Edmond 1981) and the late-stage differentiation of tholeiitic basalts (De 1974, Philpotts 1976, 1978, 1979, 1982, Biggar 1979). Also significant is the fact that liquid immiscibility has been documented both within terrestrial (Philpotts 1978) and lunar samples (Roedder & Weiblen 1971, Roedder 1978, Joliff *et al.* 1999, Shearer *et al.* 2001), and shown to occur in rocks of Archean (Coltorti *et al.* 1987, Gélinas *et al.* 1976) to recent (Philpotts 1978, 1982) age. Thus, this process is apparently relevant throughout geological time and in many magmatic environments. Also, experimental work indicates that such textures related to immiscibility can

form an equilibrium assemblage (Philpotts 1978, Visser & Koster van Groos 1979) rather than as a result of metastability (e.g., Biggar 1979).

The role of immiscibility has also been emphasized in terms of some types of ore deposits. For example, the formation of Fe–Ti–P-rich segregations due to late-stage immiscibility (Philpotts 1967, Kolker 1982) has been suggested in connection with the Kiruna deposits (Frietsch 1978, Nyström & Henriquez 1994) and the large magnetite flows of the El Laco region of northern Chile (Park 1961, Frutos *et al.* 1990, Nyström & Henriquez 1994), although this claim is not without considerable contention (e.g., Bookstrom 1995, Rhodes & Oreskes 1999, Rhodes *et al.* 1999, Naslund *et al.* 2002). Intrusive equivalents of the aforementioned include Fe–Ti–P mineralization, also known as nelsonites, in a variety of layered intrusions, including the Duluth Complex (Ripley *et al.* 1998), the Soquem Sept-Iles deposit, Quebec (McCann *et al.* 1998), anorthosite massifs (Owens & Dymek 1992, McLelland *et al.* 1994), and the Bushveld Complex (Scoon & Mitchell 1994).

The results of the present study of the Jurassic NMB of southern Nova Scotia indicate widespread development of liquid immiscibility. In the following sections, we discuss the petrological evidence, both textural and chemical, presented above in the context of immiscibility and also discuss the implications of this immiscibility in terms of some features of the NMB.

### Textural evidence for immiscibility

The definitive evidence for liquid immiscibility is the presence of two chemically distinct glasses forming globules within each other in silicate systems. Philpotts (1982) presented an authoritative summary of such criteria, as applied to basaltic rocks of various ages and settings. The Fe–Ti–P-rich globules within and in part coexisting with a felsic glass, which may be variably crystallized, so abundantly observed within the flows of the NMB, are similar to phases described by Philpotts (1982) and attributed to immiscibility. We propose the same origin for the globules and felsic glass of the NMB. Supporting this interpretation is the presence of abundant skeletal opaque grains in the mesostasis, and the absence of early-formed equant opaque minerals within the coarser, earlier-crystallized part of the sample. These textural observations point to an essential condition for immiscibility to take place, according to Philpotts (1982): the residual liquid evolved toward an Fe-rich composition, which could only occur if Fe-rich oxide phases remained soluble in the melt. In addition, Philpotts (1982) noted that “the most striking petrological feature of rocks exhibiting immiscibility is the morphology of the constituent magnetite” (p. 206), and “...no rock with magnetite phenocrysts has yet been found to contain immiscible glasses” (p. 206).

TABLE 3. REPRESENTATIVE COMPOSITIONS OF FELDSPAR IN SAMPLES OF NORTH MOUNTAIN BASALT, NOVA SCOTIA

Sample	Comments	SiO <sub>2</sub>	Al <sub>2</sub> O <sub>3</sub>	FeO	MgO	CaO	Na <sub>2</sub> O	K <sub>2</sub> O	Total	Si	Al	Fe	Ca	Na	K
<b>Plagioclase phenocrysts</b>															
19a-10	core	53.69	28.74	0.51	0.11	12.16	5.06	0.19	100.62	2.430	1.540	0.020	0.590	0.450	0.010
19a-11	rim	57.92	25.76	0.17	BD	8.81	6.20	0.32	99.42	2.620	1.370	0.000	0.420	0.540	0.020
10a-4	core	50.41	30.14	0.95	0.17	14.99	3.15	0.21	100.02	2.310	1.630	0.040	0.740	0.280	0.020
10a-5	rim	55.80	26.14	1.26	0.12	10.81	5.43	0.40	100.06	2.540	1.400	0.050	0.530	0.480	0.020
z1-99-26	core	49.18	30.20	0.76	BD	14.82	3.29	0.13	98.72	2.300	1.660	0.030	0.740	0.300	0.010
z1-99-26	core	49.22	30.50	0.49	BD	14.65	3.37	0.12	98.72	2.300	1.670	0.020	0.730	0.300	0.000
z1-99-26	rim	49.30	30.39	0.87	BD	15.02	3.34	0.15	99.34	2.290	1.660	0.030	0.740	0.300	0.010
<b>Plagioclase mesostasis</b>															
MD-08	equant	58.73	25.15	1.31	BD	8.50	6.07	0.52	100.28	2.632	1.328	0.048	0.408	0.528	0.032
MD-08	equant	58.45	25.46	1.23	BD	8.53	5.75	0.70	100.12	2.624	1.344	0.048	0.408	0.504	0.040
ZL-99-27	skeletal	57.50	25.41	1.35	0.31	8.90	5.35	0.57	99.39	2.608	1.360	0.048	0.432	0.472	0.032
z1-99-38	elongate	57.92	23.39	1.65	0.35	8.21	5.83	0.92	99.10	2.650	1.260	0.060	0.400	0.520	0.060
z1-99-38	equant	61.44	23.35	2.12	BD	7.22	6.51	0.79	101.90	2.710	1.220	0.080	0.340	0.560	0.050
<b>Feldspar overgrowth &amp; intergranular</b>															
MD-99-19	overgrowth	66.22	17.92	0.39	BD	0.31	3.26	11.54	100.03	3.024	0.960	0.016	0.016	0.288	0.672
19a-19	intergranular	64.28	18.82	0.26	BD	0.92	3.55	10.91	99.08	2.970	1.020	0.000	0.050	0.320	0.640
5a-22	intergranular	65.00	18.31	0.47	BD	0.57	2.22	12.70	100.32	2.990	0.990	0.020	0.020	0.200	0.740
MD-99-05	intergranular	64.97	18.29	0.17	BD	0.42	2.15	12.93	99.64	3.000	1.000	0.000	0.024	0.192	0.760
z1-99-26	intergranular	64.21	18.39	0.30	BD	0.28	2.32	13.54	99.36	2.980	1.010	0.010	0.020	0.210	0.800
z1-99-26	intergranular	64.26	18.52	0.36	BD	0.39	2.49	13.37	99.73	2.980	1.010	0.020	0.020	0.220	0.790

BD: below detection limit. Compositions are quoted in weight %, and in atoms per formula unit.

*Compositional evidence for immiscibility*

The composition of the relevant phases of the NMB, as determined from rastering and point analyses, is summarized in Figure 12, proposed by Philpotts (1982), which also includes the fields for the average NMB based on whole-rock compositions, the field for tholeiites with immiscible textures, and Roedder's (1951) immiscibility field for tholeiites. The following points are noted: (1) there is a distinct trend defined by the composition of the mesostasis toward the silica apex of

the diagram from the field for NMB. In addition, mesostasis compositions fall within and about the field for immiscibility; (2) the compositions of the felsic glass define a distinct field. In fact, the composition of this felsic liquid is almost identical to the average of 16 immiscible silica-rich liquids given by Philpotts (1982); (3) the subhedral, pyroxene-like phase in the mesostasis falls at the edge of or slightly within the immiscibility field (*cf.* Figs. 11, 12), and (4) the globules form a complete compositional spectrum from the edge of the immiscibility field to the Fe-Ti-Ca-P apex of the diagram.

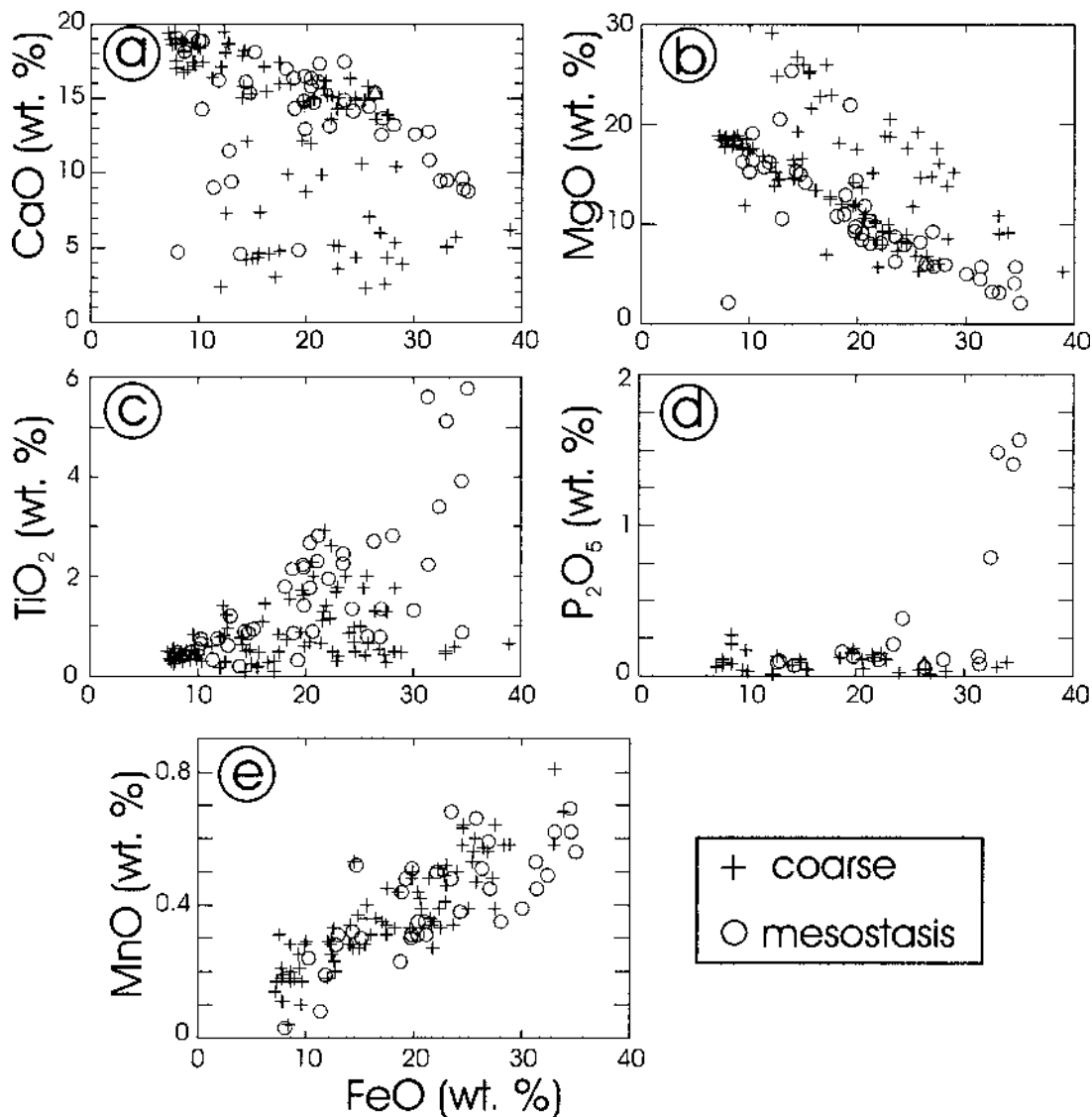


FIG. 7. Binary plots showing the composition of the pyroxenes in samples of North Mountain Basalt.

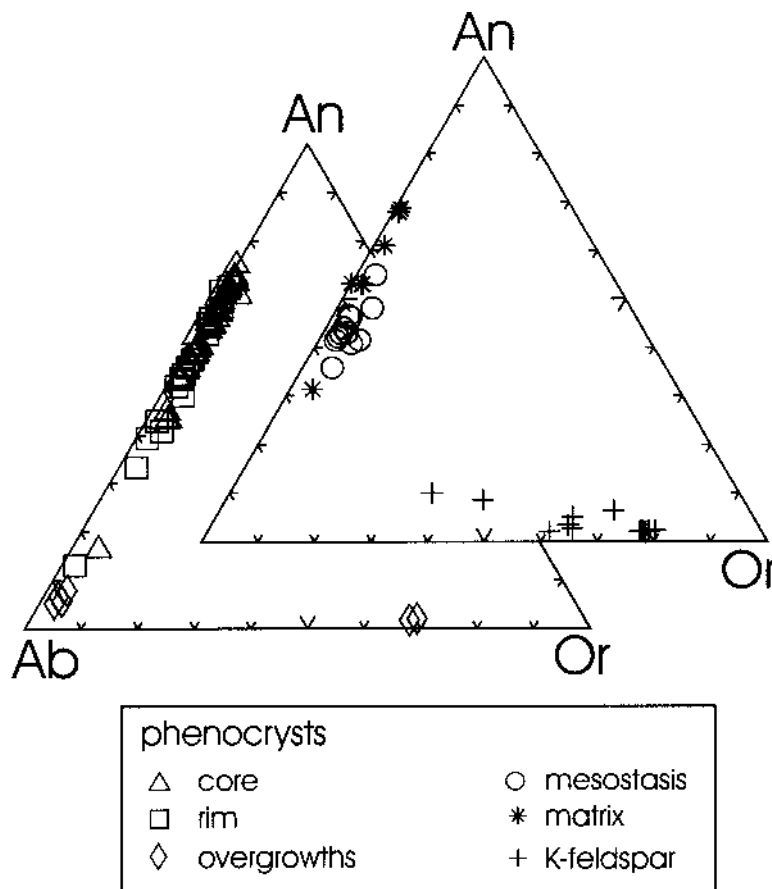


Fig. 8. Composition of the feldspars in samples of North Mountain Basalt.

The dispersion of data within and about the immiscibility field may relate to a few processes. Firstly, as noted by Philpotts (1982), the displacement of the compositions from the immiscibility fields may be due to a lower temperature of equilibration ( $<1000^{\circ}\text{C}$ ) compared to that in the synthetic system ( $1100^{\circ}\text{C}$ ) on which the field is based (Roedder 1951). Secondly, additional components, such as P and Ti, present in significant quantities in the mesostasis, expand the immiscibility field (Freestone 1978, Visser & Koster van Groos 1979). Finally, the mesostasis data track the evolution of the residual melt, which did not all undergo silicate-liquid immiscibility.

The composition of the various phases summarized in Figure 12 clearly conforms to what Philpotts (1982) has demonstrated is the result of silicate-liquid immiscibility. The data for the NMB appear to illustrate the chemical evolution of the mesostasis as it evolved toward a silica-rich liquid, which subsequently unmixing when the bulk composition of the residual liquid inter-

sected the immiscibility field. The Fe-rich component is best represented by the pyroxene-like phase, which is compositionally similar to the hedenbergite that crystallized from the Fe-rich glass identified by Philpotts (1982). On the basis of petrographic observations and chemical analysis of the mixed globules, we suggest that various amounts of subsolidus re-equilibration or unmixing have affected this pyroxene-like phase during the subsolidus cooling history of the basalts. The fact that they cooled quickly, as indicated by the abundance of various quench textures, is consistent with the texture of this phase, *i.e.*, the unmixing process was arrested prior to completion. A model for the textural evolution of this phase is shown in Figure 13.

The presence of a skeletal apatite-group mineral in the silica-rich glass and the presence of 0.3 wt.%  $\text{P}_2\text{O}_5$  in this glass are worth noting, given that Philpotts (1982) found that P is the most strongly partitioned of the elements into the mafic liquid. It is possible that the observed enrichment of P in the NMB silica-rich liquid,

TABLE 4. REPRESENTATIVE COMPOSITION OF GLOBULAR PHASES  
IN SAMPLES OF NORTH MOUNTAIN BASALT, NOVA SCOTIA

Sample	Point	SiO <sub>2</sub>	TiO <sub>2</sub>	Al <sub>2</sub> O <sub>3</sub>	FeO	MnO	MgO	CaO	Na <sub>2</sub> O	K <sub>2</sub> O	P <sub>2</sub> O <sub>5</sub>
zl-99-019	2	34.12	24.83	4.50	8.03	BD	1.04	26.46	BD	BD	0.25
zl-99-019	3	16.37	16.74	2.67	46.67	0.20	0.39	13.41	0.21	BD	2.64
zl-99-019	6	33.93	0.99	6.15	24.76	0.44	2.62	19.75	0.84	BD	10.45
zl-99-019	7	36.66	3.38	15.66	29.59	0.20	4.50	8.25	0.14	0.22	1.03
ZL-99-06C	4	7.53	14.68	1.60	69.62	<b>3.00</b>	0.63	1.87	BD	0.38	BD
ZL-99-06C	5	7.72	7.21	3.95	<b>77.44</b>	1.44	BD	0.66	0.90	0.63	BD
ZL-99-06C	6	9.57	15.53	2.87	63.72	0.77	0.52	3.35	0.14	1.10	2.05
ZL-99-09A	9	26.98	10.22	10.25	36.95	BD	1.01	7.98	1.04	1.11	4.25
ZL-99-09A	16	16.62	14.41	2.15	50.93	0.12	1.36	8.63	0.11	0.17	5.49
ZL-99-09A	18	35.92	3.76	1.47	30.77	0.77	2.40	15.35	0.40	0.14	8.66
ZL-99-09A	20	30.39	6.82	5.78	36.97	0.48	1.58	10.26	1.89	BD	5.68
ZL-99-09A	4	42.37	0.94	6.92	16.05	0.15	9.01	13.18	0.44	<b>3.38</b>	7.56
ZL-99-19	2	34.12	<b>24.83</b>	4.50	8.03	BD	1.04	<b>26.46</b>	BD	BD	0.25
ZL-99-19	3	16.37	16.74	2.67	46.67	0.20	0.39	13.41	0.21	BD	2.64
ZL-99-19	5	41.71	4.04	1.89	40.06	0.70	2.50	6.95	0.20	BD	1.65
ZL-99-19	6	33.93	0.99	6.15	24.76	0.44	2.62	19.75	0.84	BD	10.45
ZL-99-31B	20	23.66	5.76	8.26	49.22	1.06	1.31	6.85	1.22	BD	2.43
ZL-99-31B	21	31.03	9.08	<b>16.71</b>	31.46	0.74	0.90	6.48	<b>2.46</b>	0.1	1.05
ZL-99-31B	16	43.44	3.3	2.97	34.58	0.61	2.28	11.92	BD	BD	0.41
ZL-99-06C	3	47.48	1.43	2.32	27.66	0.44	3.73	16.23	BD	BD	BD
ZL-2000-B	5	<b>49.14</b>	0.52	0.81	31.03	0.68	<b>9.46</b>	8.1	BD	BD	BD
ZL-99-14	3	<b>45.45</b>	2.71	3.19	26.29	0.51	6.05	15.34	BD	BD	BD

Maximum values are recorded in bold-face font. All compositions are normalized to 100 wt.%. BD: below detection limit.

TABLE 5. REPRESENTATIVE COMPOSITIONS OF PYROXENE-LIKE PHASES  
IN SAMPLES OF NORTH MOUNTAIN BASALT, NOVA SCOTIA

Sample	SiO <sub>2</sub>	TiO <sub>2</sub>	Al <sub>2</sub> O <sub>3</sub>	FeO	MnO	MgO	CaO	P <sub>2</sub> O <sub>5</sub>
ZL-99-31B	43.44	3.30	2.97	34.58	0.61	2.28	11.92	0.41
ZL-99-06C	47.48	1.43	2.32	27.66	0.44	3.73	16.23	BD
ZL-99-09A	48.13	1.06	1.19	29.92	0.45	5.75	13.35	BD
ZL-99-09A	43.21	4.01	2.57	34.20	0.72	3.15	10.54	1.11
ZL-99-09A	47.52	1.04	1.27	33.98	0.64	3.98	11.23	BD
ZL-99-09A	46.68	1.15	1.92	34.89	0.72	2.99	11.58	BD
ZL-99-09B	49.10	0.93	3.37	34.39	0.58	4.90	6.46	BD
ZL-99-14	45.45	2.71	3.19	26.29	0.51	6.05	15.34	BD
ZL-2000-B	49.14	0.52	0.81	31.03	0.68	9.46	8.10	BD
ZL-2000-B	48.91	0.54	0.78	31.73	0.65	8.88	8.06	BD

All compositions are normalized to 100 wt.%. BD: below detection limit.

therefore, reflects rapid quenching of the melt and is a disequilibrium feature.

#### *Nature and origin of the mesostasis textures*

The variability in the textures and proportion of phases observed (crystals, glass, globules) in the meso-

stasis are considered to reflect the combined effects of the composition of the liquid at the time of quenching and the cooling rate. In the first case, the bulk composition of the mesostasis would be expected to differ after, for example, 60 and 80% crystallization of the basalt magma, hence, the mineralogy of the residual intergranular material would also reflect this. This variable

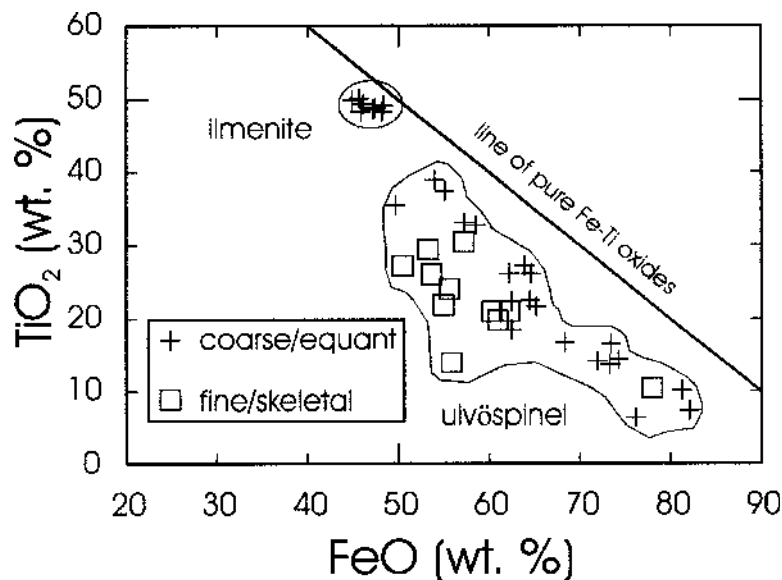


FIG. 9. Binary element plot for Fe-Ti oxides in samples of North Mountain Basalt.

is in fact illustrated by the range in the chemical composition of the mesostasis (Fig. 5), with the trend toward more silica-rich compositions tracking this progression. The second variable, cooling rate, is reflected in the variety of quench textures observed. Together, therefore, there should be a general association of mesostasis texture and bulk composition and, in fact, to a certain degree this is what one observes. For example, the best development of the mafic globules is found where there is a relative abundance of felsic glass in the mesostasis. This observation is, in fact, both consistent with and predicted by the phase diagram shown as Figure 12.

Cooling rate also is considered an important factor in formation of the immiscibility, as the relatively coarser-grained holocrystalline basalts do not contain either the felsic glass or the Fe-Ti-Ca-P-rich globules. The rapid quenching of the residual liquid would have caused rapid, disequilibrium-induced nucleation of the silicate phases, which would have driven the final liquid toward the immiscibility field. Cooling rate also was a critical factor in determining the nature of the textures formed in the mesostasis.

#### *Implications of immiscibility in the North Mountain Basalt*

We address this issue in more detail in subsequent papers in preparation, but it is nevertheless relevant to briefly refer to some obvious features in the NMB that relate to immiscibility. The first of these features is the presence of mafic pegmatites, locally pyroxenites, occurring as <1 m sills in the upper part of the massive

basalts of the lower and upper units of the NMB. The pyroxene in these rocks is Fe-rich (Greenough & Dostal 1992b, c; our data) and compositionally similar to the skeletal pyroxene in the mesostasis and the pyroxene-like phase originating from post-crystallization equilibration of the mafic globules [*i.e.*, it correspond to the Fe-rich glass of Philpotts (1982)]. Thus, we suggest that the pyroxenite sills may originated from extraction of a residual Fe-rich melt from within the flows. The occurrence of such features is of particular importance; Philpotts (1982) noted that rocks with the composition of iron-rich pyroxenite are rare, a feature that he attributed to the high specific gravity of such melts and, therefore, their tendency to sink. In the same vein, we also note the reported presence of layers of Fe-Ti oxides many meters thick in the lower part of the basal flow within a deep well drilled within the Bay of Fundy (*i.e.*, Chinampas well, D. Brown, pers. commun, 2001). This occurrence also supports the extraction of the Fe-rich melts to form distinct horizons. Is it possible that these concentrations are analogous to Kiruna Fe-Ti-P mineralization?

The second feature worth noting is the presence of thin (*i.e.*, cm scale) bands of rhyolite associated with the mafic pegmatites and pyroxenites, again in the upper parts of the lower and upper flow units (Lollis 1959, Greenough & Dostal 1992b, c, DeWolfe *et al.* 2001). Such bands may represent extracted felsic melt, which elsewhere is preserved today as silica-rich glass within the mesostasis of the basalt. The close association with the mafic pegmatites suggests a genetic association also.

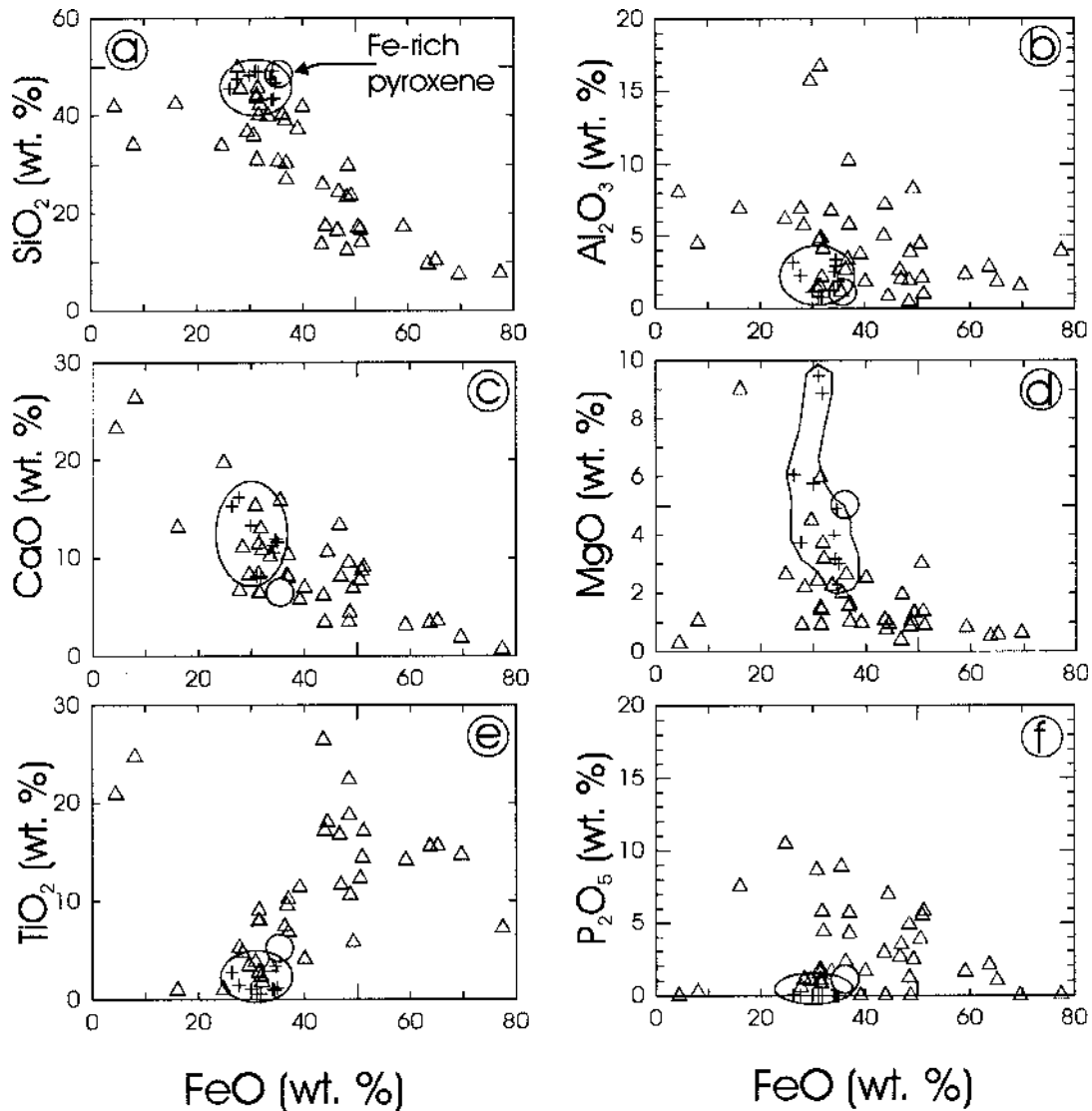


FIG. 10. Binary plots for major and minor elements in globular phases within mesostasis of samples of North Mountain Basalt. Crosses represent the pyroxene-like phase, whereas the triangles represent the brighter, Fe-Ti-P-rich phase of the globules. The circle is a representative Fe-rich pyroxene in the mesostasis that is plotted for comparison to the pyroxene-like phases.

The third feature is the presence of igneous pipes, also referred to in the literature as diktytaxitic pipes (Anderson *et al.* 1984) or segregation vesicles (Smith 1967, Anderson *et al.* 1984). These circular, elongate features occur within the lower part of the upper flow unit and are locally very abundant (5–10/m<sup>2</sup>). Work in progress indicates that the pipes are dominated by a felsic matrix with a granophyric texture containing corroded micro-scale, Fe-rich pyroxene-bearing mafic en-

claves, thus reflecting commingling of the mafic and felsic end-members of the immiscible melts within the basalts (Kontak & Dostal 2002). As interpreted by others (*e.g.*, Smith 1967, Anderson *et al.* 1984, Goff 1996), these pipes represent late-stage extraction of evolved, residual magma from the basalt magma, with subsequent migration into early-formed vesicles, perhaps formed owing to concomitant loss of volatiles from the crystallizing magma.

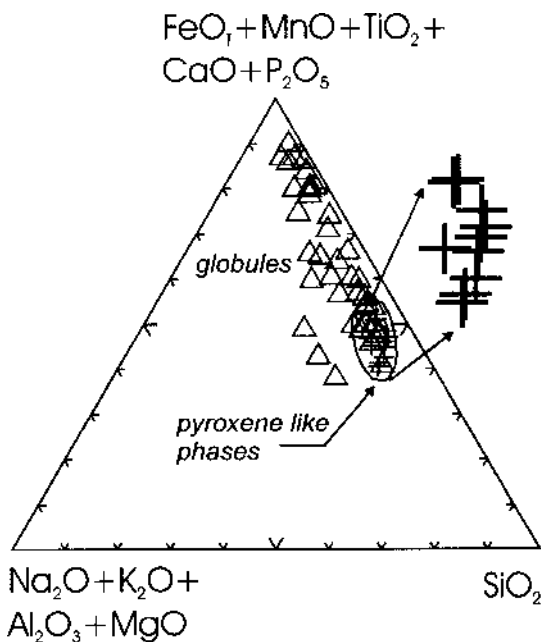


FIG. 11. Chemical composition of globular phases, plotted in terms of the diagram  $(\text{FeO} + \text{MnO} + \text{TiO}_2 + \text{CaO} + \text{P}_2\text{O}_5) - (\text{Na}_2\text{O} + \text{K}_2\text{O} + \text{Al}_2\text{O}_3 + \text{MgO}) - \text{SiO}_2$ , used by Philpotts (1982). Note that the pyroxene-like phase has a more restricted composition than the metal-rich globules. The compositions of the pyroxene-like phases are shown in greater detail with the inset.

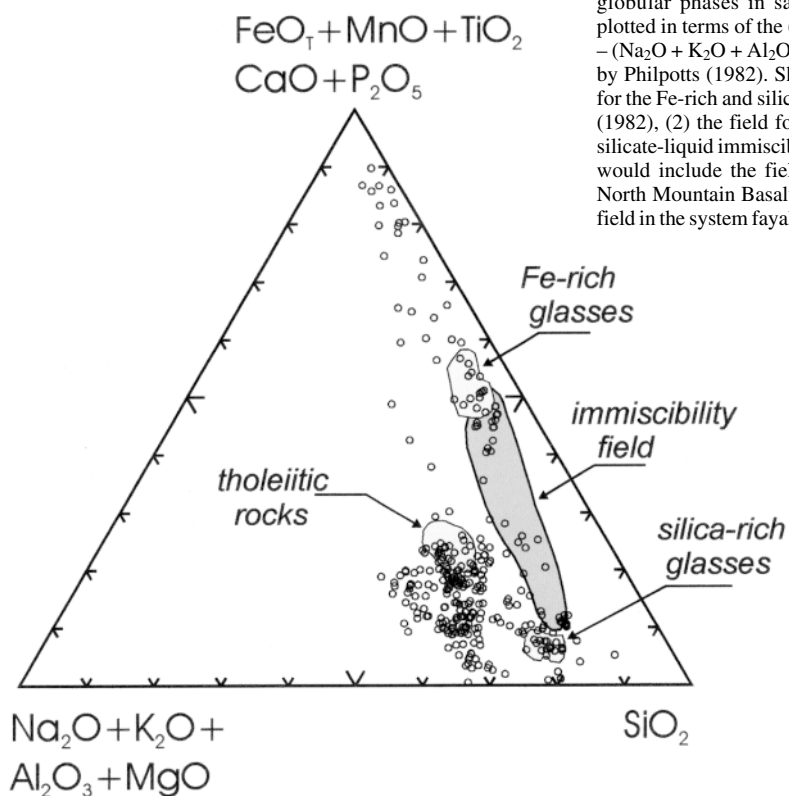


FIG. 12. Chemical compositions of the mesostasis and globular phases in samples of North Mountain Basalt plotted in terms of the  $(\text{FeO} + \text{MnO} + \text{TiO}_2 + \text{CaO} + \text{P}_2\text{O}_5) - (\text{Na}_2\text{O} + \text{K}_2\text{O} + \text{Al}_2\text{O}_3 + \text{MgO}) - \text{SiO}_2$ , the diagram used by Philpotts (1982). Shown for comparison are: (1) fields for the Fe-rich and silica-rich glasses analyzed by Philpotts (1982), (2) the field for tholeiitic rocks with evidence for silicate-liquid immiscibility [from Philpotts (1982)], which would include the field for whole-rock compositions of North Mountain Basalt samples, and (3) the immiscibility field in the system fayalite - leucite - silica (Roedder 1951).

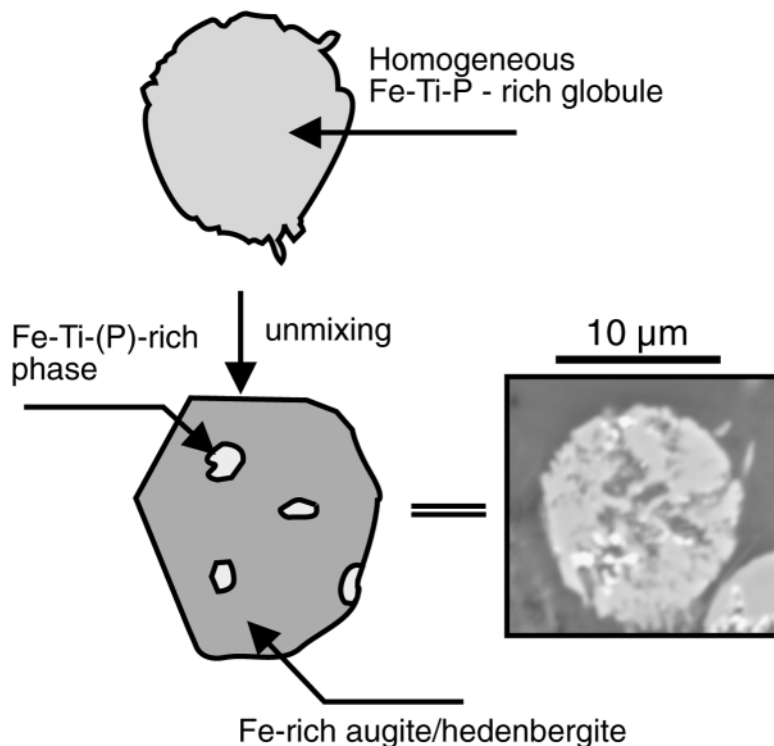


FIG. 13. Diagram summarizing schematic model for the formation of the globules occurring in mesostasis of samples of North Mountain Basalt. The homogeneous phase, initially a Fe–Ti–P-rich silicate melt, separates into a Fe–Ti–P-rich phase and Fe-rich pyroxene-type phase upon subsequent unmixing during subliquidus re-equilibration. Inset photo is a BSE image of an unmixed globule.

#### CONCLUSIONS

A detailed petrological study of the *ca.* 201 Ma North Mountain Basalt, southern Nova Scotia, has revealed that pervasive silicate-liquid immiscibility occurred during the late-stage crystallization of these quartz-normative continental tholeiitic basalts. The immiscibility occurs within a quenched mesostasis containing skeletal pyroxenes, feldspar, and Fe–Ti oxides hosted by a glass (now largely devitrified) of variable composition (basaltic to rhyolitic). The extreme development of the immiscibility is best represented by a silica-rich (*i.e.*, 70–75 wt.% SiO<sub>2</sub>) glass decorated with skeletal apatite and pyroxene, and associated Fe–Ti–P-rich globules. The globules represent an original Fe-rich melt that subsequently re-equilibrated to form an Fe-rich pyroxene (hedenbergitic) and Fe–Ti–P-rich phases. The coalescence and mobility of the immiscible melts are reflected by the presence of mafic pegmatites, rhyolitic bands, and vesicle pipes in the basalts.

#### ACKNOWLEDGEMENTS

This study was an outgrowth of work by D. Kontak on the nature and origin of zeolite mineralization in the North Mountain Basalt, carried out for the Nova Scotia Department of Natural Resources (NSDNR). The support of the NSDNR, both financial and otherwise, during this work is sincerely appreciated. Analytical work was supported by an NSERC operating grant to J. Dostal. M. DeWolfe is appreciative of the opportunity to work on the North Mountain Basalt, which was possible during summer employment (2000) with the NSDNR. The assistance of Mr. Bob McKay, Dalhousie University, with the electron-microprobe analyses and imaging facilities was instrumental to the success of this study, and we especially acknowledge his contribution. The critical reviews of the paper and insightful comments provided by H.R. Naslund, R.F. Martin and an anonymous journal reviewer are sincerely acknowledged. Finally, we note the previous work of John Greenough on aspects of the North Mountain Basalt,

which inspired this study and suggested to us that additional documentation of the petrographic features of the basalts may prove worthwhile! This paper is published with permission of the Director, NSDNR.

## REFERENCES

- ANDERSON, A.T., JR., SWIHART, G.H., ARTIOLI, G. & GEIGER, C.A. (1984): Segregation vesicles, gas filter-pressing, and igneous differentiation. *J. Geol.* **92**, 55-72.
- AUBELE, J.C., CRUMPLER, L.S. & ELSTON, W.E. (1988): Vesicle zonation and vertical structure of basalt flows. *J. Volcanol. Geotherm. Res.* **35**, 349-374.
- BIGGAR, G.M. (1979): Immiscibility in tholeiites. *Mineral. Mag.* **43**, 543-544.
- BOOKSTROM, A.A. (1995): Magmatic features of iron ores of the Kiruna type in Chile and Sweden: ore textures and magnetite geochemistry – a discussion. *Econ. Geol.* **90**, 469-473.
- BROWN, G.M. (1957): Pyroxenes from the early and middle stages of fractionation of the Skaergaard intrusion, East Greenland. *Mineral. Mag.* **31**, 511-543.
- \_\_\_\_\_ & VINCENT, E.A. (1963): Pyroxenes from the late stages of fractionation of the Skaergaard intrusion. *J. Petrol.* **4**, 175-197.
- COLTORTI, M., GIRARDI, V.A.V. & SCHORSCHER, J.H.D. (1987): Liquid immiscibility in the Archean greenstone belt of Piumhi (Minas Gerais, Brazil). *Lithos* **20**, 77-91.
- COLWELL, J.A. (1980): Zeolites in the North Mountain Basalt, Nova Scotia. *Geol. Assoc. Can. – Mineral. Assoc. Can., Field-Trip Guidebook* **18**.
- DE, A. (1974): Silicate liquid immiscibility in the Deccan traps and its petrogenetic significance. *Geol. Soc. Am., Bull.* **85**, 471-474.
- DE JONG, L.S. & OWEN, J.V. (1999): Reproducibility of electron-microprobe bulk analyses of fine-grained media: a case study using modern bone china. *Can. Mineral.* **37**, 239-246.
- DE WOLFE, M.Y., KONTAK, D.J. & DOSTAL, J.D. (2001): Documentation and implications of pervasive silicate liquid immiscibility in the Jurassic North Mountain Basalt, Nova Scotia, Canada. *Geol. Assoc. Can. – Mineral. Assoc. Can., Program Abstr.* **26**, 37.
- DIXON, S. & RUTHERFORD, M.J. (1979): Plagiogranites as late stage immiscible liquids in ophiolite and mid ocean ridge suites: an experimental study. *Earth Planet. Sci. Lett.* **45**, 45-60.
- DOSTAL, J. & DUPUY, C. (1984): Geochemistry of the North Mountain Basalts, Nova Scotia, Canada. *Chem. Geol.* **45**, 245-261.
- EBY, G.N. (1979): Mount Johnson, Quebec – an example of silicate-liquid immiscibility. *Geology* **7**, 491-494.
- \_\_\_\_\_ (1980): Minor and trace element partitioning between immiscible ocelli–matrix pairs from lamprophyre dikes and sills, Monteregian Hills petrographic province, Quebec. *Contrib. Mineral. Petrol.* **75**, 269-278.
- FREESTONE, I.C. (1978): Liquid immiscibility in alkali-rich magmas. *Chem. Geol.* **23**, 115-123.
- \_\_\_\_\_ (1979): Immiscibility in tholeiites. *Mineral. Mag.* **43**, 544-546.
- FRIETSCH, R. (1978): On the magmatic origin of iron ores of the Kiruna type. *Econ. Geol.* **73**, 478-485.
- FRUTOS, J., OYARZUN, J.M., SHIGA, Y. & ALFARO, G. (1990): The El Laco magnetite lava flow deposits, northern Chile: an up-to-date review and new data. In *Stratabound Ore Deposits in the Andes* (L. Fontboté, G.C. Amstutz, M. Cardozo, E. Cedillo & J. Frutos, eds.). Springer-Verlag, Berlin, Germany (681-690).
- GÉLINAS, L., BROOKS, C. & TRZCIENSKI, W.E., JR. (1976): Archean variolites – quenched immiscible liquids. *Can. J. Earth Sci.* **13**, 210-230.
- GOFF, F. (1996): Vesicle cylinders in vapor-differentiated basalt flows. *J. Volcanol. Geotherm. Res.* **71**, 167-185.
- GREENOUGH, J.D. & DOSTAL, J. (1992a): Cooling history and differentiation of a thick North Mountain Basalt flow (Nova Scotia, Canada). *Bull. Volcanol.* **55**, 63-73.
- \_\_\_\_\_ & \_\_\_\_\_ (1992b): Layered rhyolite bands in a thick North Mountain Basalt flow: the products of silicate liquid immiscibility. *Mineral. Mag.* **56**, 309-318.
- \_\_\_\_\_ & \_\_\_\_\_ (1992c): Geochemistry and petrogenesis of the early Mesozoic North Mountain Basalts of Nova Scotia, Canada. In *Eastern North American Mesozoic Magmatism* (J.H. Puffer & P.C. Ragland, eds.). *Geol. Soc. Am., Spec. Pap.* **268**, 149-159.
- \_\_\_\_\_, JONES, L.M. & MOSSMAN, D.J. (1989): Petrochemical and stratigraphic aspects of North Mountain basalt from the north shore of the Bay of Fundy, Nova Scotia, Canada. *Can. J. Earth Sci.* **26**, 2710-2717.
- \_\_\_\_\_ & PAPEZIK, V.S. (1987): Note on the petrology of the North Mountain basalt from the wildcat oil well Mobil Gulf Chinampas N-37, Bay of Fundy, Canada. *Can. J. Earth Sci.* **24**, 1255-1260.
- HODYCH, J.P. & DUNNING, G.R. (1992): Did the Manicouagan impact trigger end-of-Triassic mass extinction? *Geology* **20**, 51-54.
- JOLLIFF, B.L., FLOSS, C., MCCALLUM, I.S. & SCHWARTZ, J.M. (1999): Geochemistry, petrology, and cooling history of 14161,7373: a plutonic lunar sample with textural evidence of granitic fraction separation by silicate-liquid immiscibility. *Am. Mineral.* **84**, 821-837.
- KENDRICK, G.C. & EDMOND, C.L. (1981): Magma immiscibility in the Shonkin Sag and Square Butte laccoliths. *Geology* **9**, 615-619.

- KOLKER, A. (1982): Mineralogy and geochemistry of Fe–Ti oxide and apatite (nelsonite) deposits and evaluation of the liquid immiscibility hypothesis. *Econ. Geol.* **77**, 1146-1158.
- KONTAK, D.J. (2000): Nature of zeolite distribution in the North Mountain Basalt, southern Nova Scotia: field and geochemical studies. In Minerals & Energy Branch, Report of Activities 1999 (D.R. MacDonald & K. Mills, eds.). *Nova Scotia Department of Natural Resources, Rep. 2000-1*, 105-124.
- \_\_\_\_\_, & DOSTAL, J. (2002): Segregation pipes in the Jurassic North Mountain Basalts, Nova Scotia: implications for anorogenic magmatism. *Geol. Assoc. Can. – Mineral. Assoc. Can., Program Abstr.* **27**, 63.
- LOLLIS, E.W. (1959): *Geology of Digby Neck, Long Island and Brier Islands, Digby County, Nova Scotia*. Dep. of Geology, Yale Univ., unpubl. Rep.
- MALLINSON, T.J. (1986): *Petrology and Stratigraphy of the Basaltic Flows in Freeport, Long Island, Digby Co., Nova Scotia*. B.Sc. thesis, Acadia Univ., Wolfville, N.S.
- MARZOLI, A., RENNE, P. R., PICCIRILLO, E.M., ERNESTO, M., BELLINI, G. & DE MIN, A. (1999): Extensive 200-million-year-old continental flood basalts of the Central Atlantic Magmatic Province. *Science* **284**, 616-618.
- MCCANN, A.J., TRZCIENSKI, W.E., JR. & BIRKETT, T.C. (1998): The Soquem Sept-Isles Fe–Ti–P deposit. *Geol. Assoc. Can. – Mineral. Assoc. Can., Program Abstr.* **23**, A121.
- MCDUGALL, I. & HARRISON, T.M. (1988): *Geochronology and Thermochronology by the <sup>40</sup>Ar/<sup>39</sup>Ar Method*. Oxford University Press, Oxford, U.K.
- MCLELLAND, J., ASHWAL, Z. & MOORE, L. (1994): Composition and petrogenesis of oxide-, apatite-rich gabbro-norites associated with Proterozoic anorthosite massifs: examples from the Adirondack Mountains, New York. *Contrib. Mineral. Petrol.* **116**, 225-238.
- MORIMOTO, N. (1989): Nomenclature of pyroxenes. *Can. Mineral.* **27**, 143-156.
- NASLUND, H.R., HENRÍQUEZ, F., NYSTRÖM, J.O., VIVALLO, W. & DOBBS, F.M. (2002): Magmatic iron ores and associated mineralization: examples from the Chilean Andes and Coastal Cordillera. In *Hydrothermal Iron Oxide Copper–Gold and Related Deposits: a Global Perspective* (T.M. Porter, ed.). PGC Publ. Adelaide, Australia.
- NYSTRÖM, J.O. & HENRÍQUEZ, F. (1994): Magmatic features of iron ores of the Kiruna type in Chile and Sweden: ore textures and magnetite geochemistry. *Econ. Geol.* **89**, 820-839.
- OLSEN, P.E. (1988): Paleontology and paleocology of the Newark Supergroup (early Mesozoic, eastern North America). In *Triassic–Jurassic Rifting* (W. Manspeizer, ed.). Elsevier, New York, N.Y. (185-230).
- \_\_\_\_\_, SCHLISCHE, R.W. & FEDOSH, M.S. (1998): 580 ka duration of the Early Jurassic flood basalt event in eastern North America estimated using Milankovitch cyclostratigraphy. In *The Continental Jurassic* (M. Morales, ed.). *Museum of Northern Arizona Bull.* **60**, 11-22.
- \_\_\_\_\_, SHUBIN, N.H. & ANDERS, M.H. (1987): New Early Jurassic tetrapod assemblages constrain Triassic–Jurassic tetrapod extinction event. *Science* **238**, 1025-1029.
- OWENS, B.E. & DYMEK, R.F. (1992): Fe–Ti–P-rich rocks and massif anorthosite: problems of interpretation illustrated from the Labrieville and St. Urbain plutons, Quebec. *Can. Mineral.* **30**, 163-190.
- PAPEZIK, V.S., GREENOUGH, J.D., COLWELL, J.A. & MALLINSON, T.J. (1988): North Mountain basalt from Digby, Nova Scotia: models for a fissure eruption from stratigraphy and petrochemistry. *Can. J. Earth Sci.* **25**, 74-83.
- PARK, C.F., JR. (1961): A magnetite “flow” in northern Chile. *Econ. Geol.* **56**, 431-436.
- PE-PIPER, G. (2001): Mode of occurrence, chemical variation and genesis of mordenite and associated zeolites, Morden area, Nova Scotia, Canada. *Can. Mineral.* **38**, 1215-1232.
- \_\_\_\_\_, JANSA, L.F. & LAMBERT, R.ST.J. (1992): Early Mesozoic magmatism on the eastern Canadian margin: petrogenetic and tectonic significance. In *Eastern North American Mesozoic Magmatism* (J.H. Puffer & P.C. Ragland, eds.). *Geol. Soc. Am., Spec. Pap.* **268**, 13-36.
- PHILPOTTS, A.R. (1967): Origin of certain iron–titanium oxide and apatite rocks. *Econ. Geol.* **62**, 303-315.
- \_\_\_\_\_, (1976): Silicate liquid immiscibility: its probable extent and petrogenetic significance. *Am. J. Sci.* **276**, 1147-1177.
- \_\_\_\_\_, (1978): Textural evidence for liquid immiscibility in tholeiites. *Mineral. Mag.* **42**, 417-425.
- \_\_\_\_\_, (1979): Silicate liquid immiscibility in tholeiitic basalts. *J. Petrol.* **20**, 99-118.
- \_\_\_\_\_, (1981): Liquid immiscibility in silicate melt inclusions in plagioclase phenocrysts. *Bull. Minéral.* **104**, 317-324.
- \_\_\_\_\_, (1982): Compositions of immiscible liquids in volcanic rocks. *Contrib. Mineral. Petrol.* **80**, 201-218.
- \_\_\_\_\_, & HODGSON, C.J. (1968): Role of liquid immiscibility in alkaline rock genesis. *Int. Geol. Congress, 23<sup>rd</sup> (Prague)* **2**, 175-188.
- RHODES, A.L. & ORESKES, N. (1999): Oxygen isotope composition of magnetite deposits at El Laco, Chile: evidence of formation from isotopically heavy fluids. In *Geology of Ore Deposits of the Central Andes* (B.J. Skinner, ed.). *Soc. Econ. Geol., Spec. Publ.* **7**, 333-351.

- \_\_\_\_\_, \_\_\_\_\_ & SHEETS, S.A. (1999): Geology and rarer earth element geochemistry of magnetite deposits at El Laco, Chile. *In* *Geology and Ore Deposits of the Central Andes* (B.J. Skinner, ed.). *Soc. Econ. Geol., Spec. Publ.* **7**, 299-332.
- RIPLEY, E.M., SEVERSON, M.J. & HAUCK, S.A. (1998): Evidence for sulfide and Fe-Ti-P-rich liquid immiscibility in the Duluth Complex, Minnesota. *Econ. Geol.* **93**, 1052-1062.
- ROBINSON, P. (1980): The composition space of terrestrial pyroxenes – internal and external limits. *In* *Pyroxenes* (C.T. Prewitt, ed.). *Rev. Mineral.* **7**, 419-494.
- ROEDDER, E. (1951): Low temperature liquid immiscibility in the system  $K_2O-FeO-Al_2O_3-SiO_2$ . *Am. Mineral.* **36**, 282-286.
- \_\_\_\_\_ (1978): Silicate liquid immiscibility in magmas and in the system  $K_2O-FeO-Al_2O_3-SiO_2$ : an example of serendipity. *Geochim. Cosmochim. Acta* **42**, 1597-1617.
- \_\_\_\_\_ & WEIBLEN, P.W. (1971): Petrology of silicate melt inclusions, Apollo 11 and 12, and terrestrial equivalents. *In* *Second Lunar Science Conference Proceedings*. *Geochim. Cosmochim. Acta, Suppl.* **2**, 2, 507-528.
- SCOON, R.N. & MITCHELL, A.A. (1994): Discordant iron-rich ultramafic pegmatites in the Bushveld Complex and their relationship to iron-rich intercumulus and residual liquids. *J. Petrol.* **35**, 881-917.
- SHEARER, C.K., PAPIKE, J.J. & SPILDE, M.N. (2001): Trace-element partitioning between immiscible lunar melts: an example from naturally occurring lunar melt inclusions. *Am. Mineral.* **86**, 238-246.
- SMITH, R.E. (1967): Segregation vesicles in basaltic lava. *Am. J. Sci.* **265**, 696-713.
- STEVENS, G.R. (1980): Mesozoic volcanism and structure, northern Bay of Fundy region, Nova Scotia. *Geol. Assoc. Can. – Mineral. Assoc. Can., Field-Trip Guidebook* **18**.
- VISSER, W. & KOSTER VAN GROOS, A.F. (1976): Liquid immiscibility in  $K_2O-FeO-Al_2O_3-SiO_2$  – a reply. *Nature* **264**, 426-427.
- \_\_\_\_\_ & \_\_\_\_\_ (1979): Phase relations in the system  $K_2O-FeO-Al_2O_3-SiO_2$  at 1 atmosphere with special emphasis on low temperature liquid immiscibility. *Am. J. Sci.* **279**, 70-91.
- WARK, J.M. & CLARKE, D.B. (1980): Geochemical discriminators and the palaeotectonic environment of the North Mountain basalts, Nova Scotia. *Can. J. Earth Sci.* **17**, 1740-1745.

*Received February 1, 2002, revised manuscript accepted July 17, 2002.*